The following statement is placed here in accordance with the American Meteorological Society copyright policy.

© 2020 American Meteorological Society (AMS). For permission to reuse any portion of this work, please contact permissions@ametsoc.org. Any use of material in this work that is determined to be "fair use" under Section 107 of the U.S. Copyright Act (17 U.S. Code §107) or that satisfies the conditions specified in Section 108 of the U.S. Copyright Act (17 USC §108) does not require the AMS's permission. Republication, systematic reproduction, posting in electronic form, such as on a website or in a searchable database, or other uses of this material, except as exempted by the above statement, requires written permission or a license from the AMS. All AMS journals and monograph publications are registered with the Copyright Clearance Center (https://www.copyright.com). Additional details are provided in the AMS Copyright Policy statement, available on the AMS website (https://www.ametsoc.org/PUBSCopyrightPolicy).

The Regeneration of the Lofoten Vortex through Vertical Alignment

MARTA TRODAHL

University of Oslo, Oslo, Norway

PÅL ERIK ISACHSEN

University of Oslo, and Norwegian Meteorological Institute, Oslo, Norway

JONATHAN M. LILLY

Theiss Research, La Jolla, California

JOHAN NILSSON

Stockholm University, Stockholm, Sweden

NILS MELSOM KRISTENSEN

Norwegian Meteorological Institute, Oslo, Norway

(Manuscript received 13 February 2020, in final form 29 June 2020)

ABSTRACT

Observations from the past decades have promoted the idea of a long-lived anticyclonic vortex residing in the Lofoten Basin. Despite repeatedly recorded intense anticyclones, the observations cannot firmly decide whether the signature is of a single vortex or a succession of ephemeral vortices. A vortex persisting for decades requires some reinvigoration mechanism. Wintertime convection and vortex merging have been proposed candidates. We examine Lofoten Basin vortex dynamics using a high-resolution regional ocean model. The model is initialized from a coarser state with a weak eddy field. The slope current intensifies and sheds anticyclonic eddies that drift into the basin. After half a year, an anticyclone arrives at the center, providing the nucleus for a vortex that remains distinct throughout the simulation. Analyses show that this vortex is regenerated by repeated absorption and vertical stacking of lighter anticyclones. This compresses and—in concert with potential vorticity conservation—intensifies the combined vortex, which becomes more vertically stratified and also expels some fluid in the process. Wintertime convection serves mainly to vertically homogenize and densify the vortex, rather than intensifying it. Further, topographic guiding of anticyclones shed from the continental slope is vital for the existence and reinvigoration of the Lofoten vortex. These results offer a new perspective on the regeneration of oceanic anticyclones. In this scenario the Lofoten vortex is maintained through repeated merging events. Fluid remains gradually exchanged, although the vortex is identifiable as a persistent extremum in potential vorticity.

1. Introduction

The Lofoten Basin is distinct within the Nordic seas in that the region is exceptionally rich in mesoscale vortices. The vortex field is dominated by large, buoyant anticyclones originating from the unstable Norwegian Atlantic Current (NwAC) flowing along the Norwegian coast. The eddy shedding from the boundary current is responsible for spreading Atlantic Water (AW) away from the coast, making the basin also significantly warmer than the surrounding seas. The Lofoten Basin thus stands out as a hot spot in maps of both sea surface temperatures (SST) and eddy kinetic energy (EKE). The study area is indicated in Fig. 1. Shown are observed time-mean SSTs extracted from the Operational SST and Sea Ice Analysis (OSTIA) reanalysis (Donlon et al. 2012) as well as time-mean geostrophic surface currents estimated by differentiating the altimetric mean dynamic topography produced by AVISO. Warm, saline AW enters the Nordic Seas and is carried northward

Corresponding author: Marta Trodahl, marta.trodahl@geo.uio.no

DOI: 10.1175/JPO-D-20-0029.1

© 2020 American Meteorological Society. For information regarding reuse of this content and general copyright information, consult the AMS Copyright Policy (www.ametsoc.org/PUBSReuseLicenses).

Unauthenticated | Downloaded 02/18/21 11:07 AM UTC

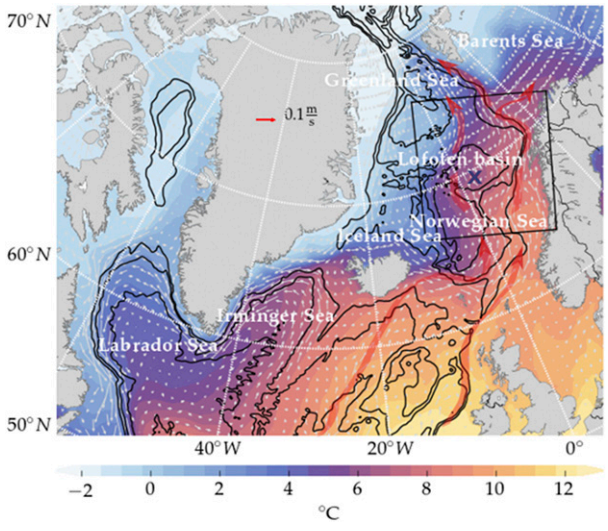

FIG. 1. Time-mean SSTs (°C) from the OSTIA reanalysis. Vectors show time-mean surface geostrophic currents, provided by AVISO. The study region is marked by the black box, and the observed Lofoten vortex time-mean position by the blue cross. Topography is shown in black contours for every 1000 m. The red lines show approximate paths taken by the NwAC.

toward the Arctic Ocean. On its journey the AW experiences heat loss to the atmosphere and progressively densifies (Mauritzen 1996). Through eddy activity the residence time of AW in these areas of major atmospheric heat loss is prolonged. The longest residence time of AW, about 1–3 years, is thought to occur in the Lofoten Basin (Gascard and Mork 2008).

In addition to being infused by transitory turbulent mesoscale features, the Lofoten Basin is home to a uniquely persistent anticyclonic vortex. Oceanographic observations gathered during the time span 1970–90 revealed the presence of a large, persistent high pressure perturbation in the central part of the basin (Ivanov and Korablev 1995a). Later studies have confirmed the presence of this high pressure feature which is commonly referred to as the Lofoten vortex (LV). What makes this one vortex remarkable compared with other vortices is that it somehow manages to sustain its coherence in a violent deformation field for long periods of time. Coherent mesoscale eddies in the ocean typically have lifetimes of days to months. The LV, however, leaves an imprint on decadal time-mean sea surface height (SSH) fields. This imprint suggests an exceptionally long-lived mesoscale vortex, observed perhaps nowhere else in the World Ocean. The dynamics providing such a resilience to vortex breakup presents a puzzle and has been the subject of considerable scientific attention over the last few decades. Søiland et al. (2016) speculate that the vortex lifetime may even extend beyond the five decades of available observational data.

Long-lived vortices are rare but have been observed elsewhere. A prevalence of large anticyclones is found on Jupiter and Saturn. Notably, the Great Red Spot in the Jovian atmosphere is an anticyclonic vortex that has survived for over 300 years (Nezlin et al. 1993). In the Argentine Basin, float trajectories and satellite altimetry have recorded a permanent, stationary anticyclone, the Zapiola Anticyclone (de Miranda et al. 1999). This vortex is, however, not analogous to the LV as it is driven by completely different dynamics. While the LV is situated in the deepest parts of a topographic depression, the Zapiola Anticyclone is a barotropic feature with a circulation forced to follow closed potential vorticity contours over a topographic rise (de Miranda et al. 1999). Another anticyclonic recirculation considered to be a quasi-permanent feature is the Mann Eddy, found along the path of the North Atlantic Current in the central Newfoundland Basin (Mann 1967; Meinen 2001). The persistence of the Mann Eddy is evidenced by its sea surface signature showing up in altimetry climatologies. Still, the dynamics of this vortex has not been meticulously examined up until the recent high-resolution (2.5 km) model study of Solodoch et al. (2020), the study also facilitates existing hydrographic and altimetry data to complement the model data. Unlike the LV, the Mann Eddy is surface intensified but similarly resides within a topographic depression in which it drifts. Mergers are found to assist in sustaining the vortex and its origins takes place within the depression. Perhaps more closely related to the LV, long-lived vortices have been observed as bulges within and below the thermocline in various regions of the World Ocean (Prater and Sanford 1994). These vortices are as a rule all anticyclones. A typical intrathermoclinic (ITV) or subthermoclinic vortex (STV) has a lens-like shape and an anomalous core with small vertical changes in water properties that stands out against the background stratification. The most well-known example of this type of vortices are Mediterranean water eddies (meddies). If they do not encounter a major seamount, meddies may dissipate slowly and stay intact for several years, some estimated from observations to last up to 5 years (Richardson et al. 2000). However, the same study estimated that about 90% out of 27 meddies analyzed, did collide with seamounts that led them to disintegrate. These collisions were found to occur on average 1.7 years after a meddy formation.

Observations show that the LV share similarities with subthermocline/intrathermocline anticyclonic vortices reported from other oceanic regions. The core consists

Unauthenticated | Downloaded 02/18/21 11:07 AM UTC

of a weakly stratified, fast-spinning water mass anomalous with respect to its surroundings.[1] The core depth is centered at about 700–900 m and the typical radius at which the maximum azimuthal velocity occurs is 15–30 km (Yu et al. 2017). The vortex commonly resides within the 3000-m isobath, near 3°E and 69.5°–70°N (Rossby et al. 2009; Søiland and Rossby 2013; Fer et al. 2018). The observed time-mean vortex position is indicated by a blue cross in Fig. 1.

Fer et al. (2018) report a maximum azimuthal speed of 0.8 m s^{-1} at 950 m depth. The momentum balance of the core is highly nonlinear, with the relative vorticity estimated from the observed flow field typically around $-0.5f$ but reaching as low as $-0.9f$ ($f = 1.37 \times 10^{-4}$ being the Coriolis parameter at 70°N) near the eddy axis, which is close to the theoretical limit for anticyclones of $-f$ (Fer et al. 2018).

A continuous rejuvenation of the vortex is apparently needed to sustain such levels of intensity in an otherwise violent environment with high deformation rates as well as dissipation from e.g., bottom friction. Two hypotheses have been previously proposed for the maintenance of the vortex. Using observational data, Ivanov and Korablev (1995a,b) suggested that wintertime convection plays a key role. They postulate that convection events lead to a deepening of the isopycnals below the vortex core, causing the azimuthal velocity to intensify through the increased radial density gradient. However, in a later model study, Köhl (2007) suggested that anticyclonic eddies generated from the unstable boundary current propagate westward and are attracted to center of the basin by nonlinear drift under the topographic beta effect. The accumulation of anticyclones in the center of the relatively small Lofoten Basin encourages the mergers of like-signed vortices. Thus in this hypothesis, the slope eddies drift toward the Lofoten vortex and energize it through a merging process. In this study we will look closer at the merging hypothesis. We do not investigate meticulously the role played by convection, but recognize that it may affect the rejuvenation process.

Obtaining detailed observations of vortex mergers is an immense challenge. The process has limited predictability and happens on a very short time scale. Observations that have captured vortex interactions are few, and only sporadic accounts exist from in situ observations. Due to the challenges in obtaining sufficient amount of observational data, investigations of vortex mergers have more commonly been conducted in various numerical and theoretical settings. Many experiments consider idealized circumstances where the interacting vortices are studied in isolation with only some active processes. These idealized choices are imperative in order to assess how a merger is impacted by specific influences, such as external strain, stratification, and asymmetric vortex properties. The majority of theoretical works consider interactions of symmetric anticyclones that share the same strength and density, with cores situated on the same vertical level. But a much more realistic scenario is where the vortices are not necessarily similar in size, strength nor density.

One of the first records of a vortex coalescence was taken off the East Australian Current (Cresswell 1982). Two anticyclones at different depths coalesced by aligning vertically over the course of 20 days. Partly motivated by the observations of Cresswell (1982) and Nof and Dewar (1994) studied the interaction of two anticyclonic lenses having different densities. Using laboratory and numerical experiments, they found that the lenses are inclined to align vertically rather than undergoing a horizontal merger where a substantial amount of the two vortex cores melt together to form a single, larger vortex. When interacting, the lenses seek a final state where one is placed on top of the other. The lighter vortex slides on top of the denser vortex, resulting in a dual core vertical structure. The notion of vertical alignment was first presented by McWilliams (1990) in a study of decaying stratified 3D quasigeostrophic turbulence, where vortices in the end state largely appeared to be stacked on top of each other in elongated vertical structures. Sparked by these results, Polvani (1991) studied the process analytically in a quasigeostrophic two-layer system. He found that two vortices from different density classes coalesce by vertically aligning only if their radii are on the order of or larger than the Rossby deformation radius.

Over the years, an increasing observational record of dual core anticyclones emerged (Cresswell 1982; Bogdanov et al. 1985; Belkin and Mikhailitchenko 1986; Armi et al. 1989; Brundage and Dugan 1986; Prater and Sanford 1994; Schultz Tokos et al. 1994; Lilly et al. 2003; Rogachev et al. 2007; Dmitrenko et al. 2008; Itoh and Yasuda 2010; Carton et al. 2010; Baird and Ridgway 2012; Barceló-Llull et al. 2017; Garreau et al. 2018; Belkin et al. 2020). While the limited amount of data does not give direct evidence that these double cores arise from vertical alignment, several studies hypothesize that this could be the case. In an eddy census from the Labrador Sea, Lilly et al. (2003) found a strong dominance of anticyclonic vortices. The observed anticyclones were grouped into two categories, surface-intensified Irminger rings and middepth-intensified ''convective lens'' type eddies. Among both types of anticyclones, several exhibited vertically aligned cores. The hydrographic signature of the cores strongly suggested that they originated from

[1] Figure 7 shows time-mean profiles of the model simulated LV, which reproduces main observational features.

Unauthenticated | Downloaded 02/18/21 11:07 AM UTC

two initially separated eddies, rather than originating from, e.g., wintertime convection. The study concluded that the only tenable mechanism of joining the two cores was through vertical alignment.

Observations have also revealed that the Lofoten vortex core does at times have a dual core structure (Yu et al. 2017; Fer et al. 2018). In this paper, we study the mesoscale eddy field in the Lofoten Basin, with the focus on the regeneration mechanism of the LV. Specifically, we revisit the hypothesis of Köhl (2007) and investigate the role of vortex mergers. Benefiting from a model with unprecedentedly high temporal and spatial resolution, we bring new insights to this discussion by studying vortex interactions in detail. We investigate whether the observed occasional double-core structure of the LV may result from the kinds of vortex coalescence discussed by Nof and Dewar (1994). We find that vertical alignment episodes are indeed occurring, and moreover we find that these are common not only for the LV, but also for Lofoten Basin anticyclonic vortices in general. The vortices resident in the basin have generally been subject to different cooling and warming periods, and have originated in different seasons, and consequently reside at different vertical levels. We will give a high-resolution account of how merger events with the LV play out in a realistic setting with all complexity of the flow field present. The net result strongly supports the hypothesis that a vortex merger is the primary mechanism for the regeneration if the LV.

2. Data and methods

a. Model

Our study employs a numerical simulation using the Regional Ocean Modeling System (ROMS; Shchepetkin and McWilliams 2005; Haidvogel et al. 2008). ROMS is a hydrostatic, primitive equation model formulated with a horizontal near-orthogonal staggered C grid and a vertical coordinate system, called the *s* coordinate (Shchepetkin and McWilliams 2005), in which the model layers follow the variations of the seabed terrain. The model domain is shown in Fig. 1.

The model's lateral grid spacing is 800 m. At this resolution, mesoscale eddies on the scale of the internal Rossby deformation radius of about 6–7 km would be well resolved throughout the domain, except on the very shallow parts of the continental shelf. The vertical grid consists of 60 layers distributed so as to obtain a finer resolution near the surface. The vertical spacing is at a minimum 0.3 m near the surface and up to 80 m in the bottom layers. A fourth-order centered scheme is used for vertical advection, and a third-order upwind scheme is used for horizontal advection. No explicit horizontal eddy viscosity or diffusion is applied, but the upwind advection scheme includes some implicit biharmonic diffusion. The k–ε version of the general length scale (GLS) scheme is employed for small-scale vertical mixing (Umlauf and Burchard 2003; Warner et al. 2005). The open lateral boundaries are relaxed toward the global Forecast Ocean Assimilation Model (FOAM; MacLachlan et al. 2015) with a 15-day relaxation time scale, and atmospheric forcing is taken from the ERA-interim atmospheric reanalysis (Uppala et al. 2005). Runoff from major rivers are supplied by monthly climatologies from a river discharge model from the Norwegian Water Resources and Energy Directorate (Beldring et al. 2003).

The model is started in January 1993 and run for 10 years. The initial model state is given by FOAM, which has a resolution of 25 km. After two years of spinup, the last 8 years of the model simulation (1995–2003) are analyzed to ensure that the dynamics are consistent with the boundary conditions. Model output is stored every 6 h. For parts of the analysis we use daily mean fields, whereby tides and other motions excited by fast atmospheric forcing are mostly filtered out. Nevertheless, a high temporal resolution was found to be necessary to capture the details of the eddy interactions, so merging processes are studied with the 6-hourly model fields.

Figure 2 shows the time-mean SST and surface flow field extracted from observations [the Climatological Atlas of the Nordic Seas and Northern North Atlantic (1950–2012) (Korablev et al. 2014) and AVISO] and also the model. The model contains finer structures than the observations, reflecting the coarser effective resolution of the observational dataset. However, the general structure of the two fields agree well. The model captures the Mohn Ridge frontal zone as well as the warm water carried by the Norwegian Atlantic Current closer to the coast. A discrepancy between the observations and the model is seen north of the Lofoten Basin, around 5°–10°E and 72°N, where the model exhibits a tongue of cold water. This feature is seen in the wintertime observational data but is less prominent in the annual mean fields. The apparent lack of a cold tongue in the observations may plausibly be related to resolution or under sampling during winter. In the model, this feature seems to arise due to the steering of the time-mean current along the bottom topography. Alternatively, this might indicate that the model currents are too constrained by topography, an effect not uncommon in models with terrain-following vertical coordinate systems (Haney 1991).

Estimates of geostrophic surface EKE from satellite altimetry data (AVISO) and model are given in Figs. 2c

Unauthenticated | Downloaded 02/18/21 11:07 AM UTC

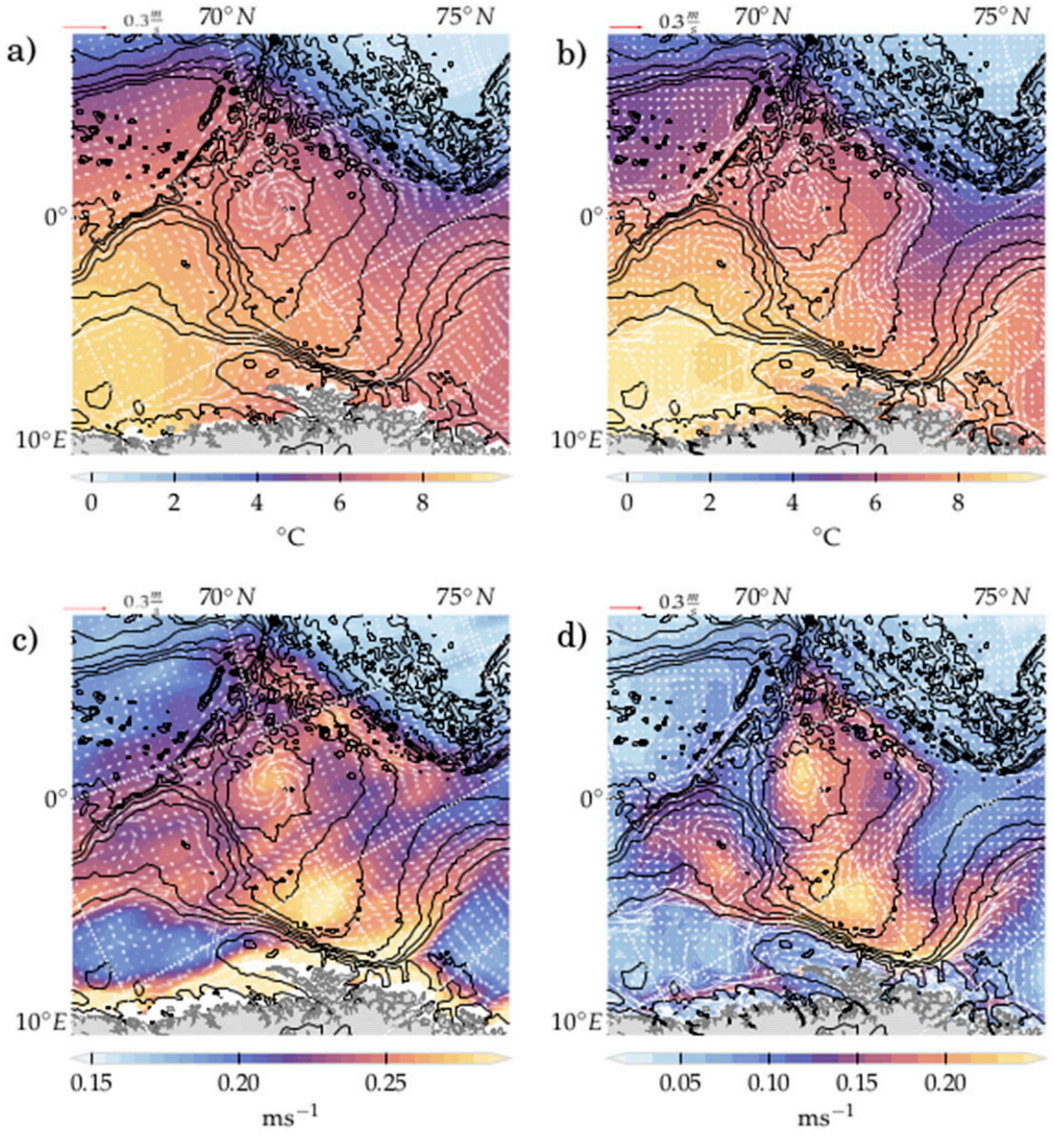

FIG. 2. Time-mean SSTs (°C) from (a) the Climatological Atlas of the Nordic Seas and Northern North Atlantic (1950–2012) and (b) model (1995–2002), together with square root of geostrophic EKE (m s^{-1}) obtained by differentiating along-track SSH anomalies provided by (c) AVISO and (d) the model. Vectors show time-mean surface geostrophic currents. Topography is shown with black contours in this and subsequent maps with 500-m increments, starting at the 200-m depth contour.

and 2d. The altimeter data contains instrumental noise, which produces artificially high EKE levels at high wavenumbers (Le Traon et al. 1990). This is likely responsible for a general higher EKE level in the observations compared to the model, as seen especially in relatively quiescent regions in the model. However, the main observed spatial patterns of variability are well captured by the model, including the EKE tongue extending from the steep slope region off the Lofoten Islands (around 10°–12°E and 68°N). Model EKE levels in the Lofoten Basin are close to those of the observations, giving us confidence in the eddy dynamics represented in the model.

b. Eddy detection

We extract coherent mesoscale vortices from the model flow field using the eddy detection method of Penven et al. (2005) (for more details see the appendix). This method is based on the facts that a coherent vortex is a pressure perturbation with closed streamlines around its center and that the interior of a coherent vortex is characterized by strong relative vorticity. By

Unauthenticated | Downloaded 02/18/21 11:07 AM UTC

contrast, the boundary of the vortex, as well as the regions between separated vortices, are typically subject to large deformation rates. The method used is a hybrid scheme that involves locating closed contours of both SSH and of the Okubo–Weiss (OW) parameter (see Fig. 3). The OW parameter compares the strength of deformation to that of rotational motion taking the form

$$\mathrm{OW} = S_n^2 + S_s^2 - \zeta^2, \tag{1}$$

where the normal strain $S_n = \partial_x u - \partial_y v$ and shear strain $S_s = \partial_x v + \partial_y u$ measure the fluid deformation, while relative vorticity $\zeta = \partial_x v - \partial_y u$ represents rotation of the fluid about a vertical axis. Essentially, regions in the flow field where $\mathrm{OW} \lesssim 0$ are potentially coherent eddy cores. Although the OW parameter was originally designed to identify coherent structures in idealized 2D turbulent flows, it is also commonly applied to identify vortices in more realistic geophysical flows (Isern-Fontanet et al. 2003; Penven et al. 2005; Chelton et al. 2007). For detection purposes, we use the OW contour calculated from horizontal velocities at 100-m depth. We chose to do the detection a bit below the surface to avoid some noise in the OW parameter. Computing the OW directly at the surface produces more small-scale noise.

3. Results

a. Model spinup

The model is initialized from FOAM fields interpolated to the model grid from lateral resolution of 25 km. The dynamical inconsistencies caused by the interpolation give rise to an initial shock creating some domain-wide gridscale noise. However, it takes less than a week before this shock has settled and the noise is smoothed out.

The deformation radius ($\int_{-H}^{0} N dz/f$), where N is the square root of the buoyancy frequency computed using the ambient density field, in the area ranges from 2 to 8 km (as shown in Fig. 7a). Hence, the initial state drawn from a coarse model that has a weak mesoscale eddy field and no identifiable Lofoten vortex. Once the higher-resolution ROMS model begins running, the Norwegian Atlantic Slope Current (NwASC) off the Lofoten Islands quickly intensifies and via instabilities becomes a source of anticyclonic eddies that move into and energize the relatively quiescent initial model state in the Lofoten Basin. Figure 4 shows a snapshot of 1) model temperature and 2) at 400-m depth in the basin, one month into the simulation. No large anticyclones have reached the central Lofoten Basin at this point, the LV has not appeared yet. Originating from the slope, anticyclones shed from the NwAC trap and carry warm Atlantic water in their

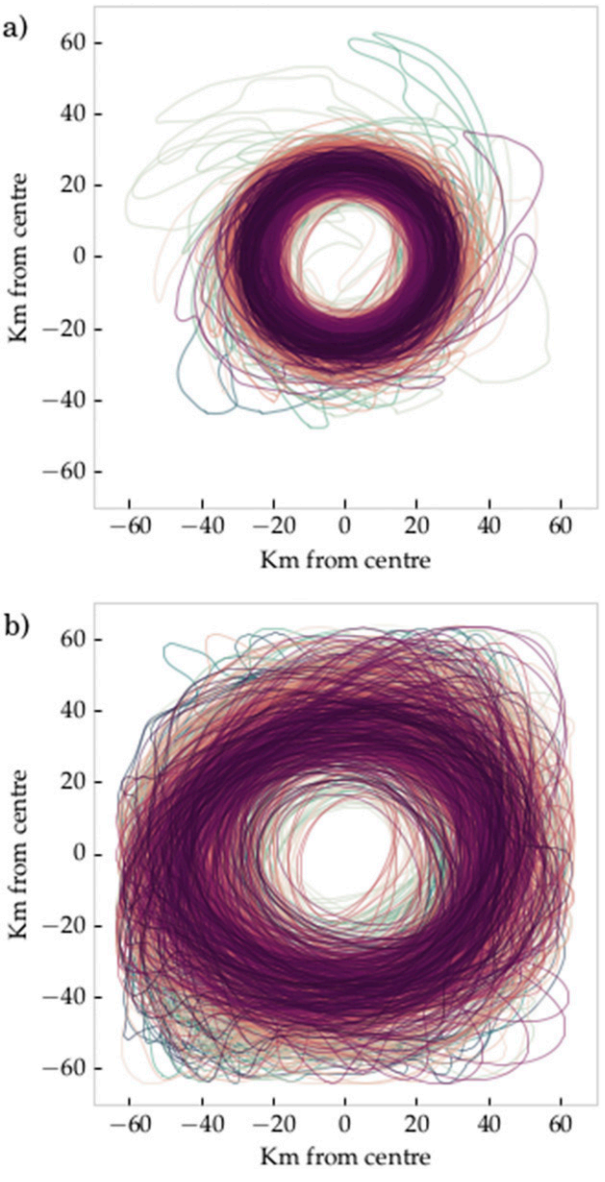

FIG. 3. (a) OW = 0 contours and (b) outermost SSH contour extracted daily around the LV center found each day during 1995–99, the first 4 years after the spinup period. Colors are arbitrary.

cores. The lateral westward spread of this water mass is readily seen in the figure.

As time proceeds, more slope anticyclones reach the central basin, which then accumulate there. At later stages in the simulation, the basin hydrography has undergone a substantial modification compared to the initial field. Figure 5a shows a vertical transect through the basin from the initial model state, the 15 January 1994. Figure 5b shows the same transect at the same date 8 years into the simulation. The fine resolution of the ROMS model produces sharper fronts and slender boundary currents. The initially broad NwAC is now

Unauthenticated | Downloaded 02/18/21 11:07 AM UTC

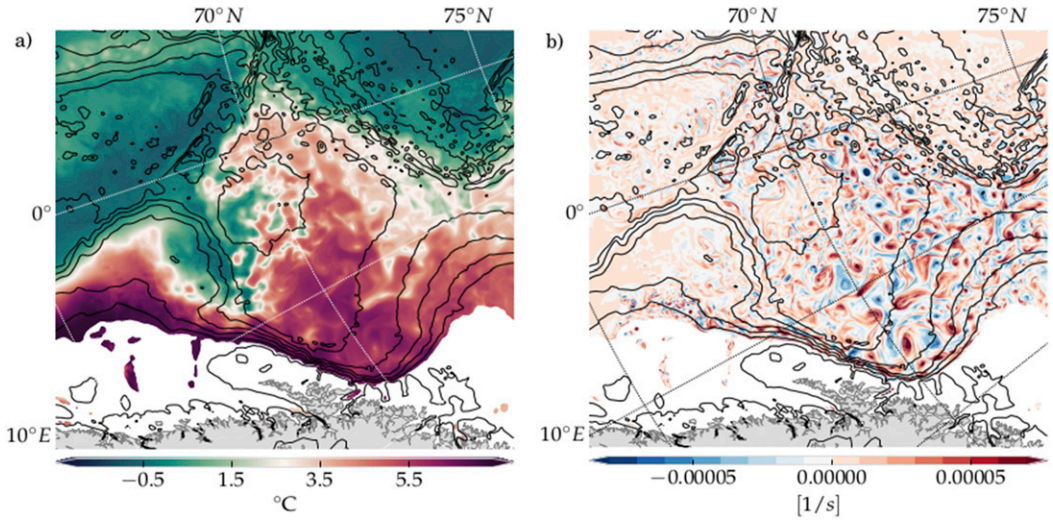

FIG. 4. Snapshot of (a) model temperature and (b) relative vorticity at 400-m depth on the 1 Feb 1994, one month after initialization. White areas are shallower than 400 m.

confined to the continental slope, in agreement with observations showing current width on the order of tens of kilometer (Orvik and Niiler 2002; Rodionov et al. 2004). The observed vertical extent of the AW typically lies between 500 and 700 m (Yu et al. 2017). The AW, with salinity above 35 psu and temperatures above 3°C, occupied the top 400 m at the start of the simulation, and later occupies the top 700 m. This indicates that when the high-resolution and eddy-rich simulation is initialized from the coarser model fields with a weaker eddy

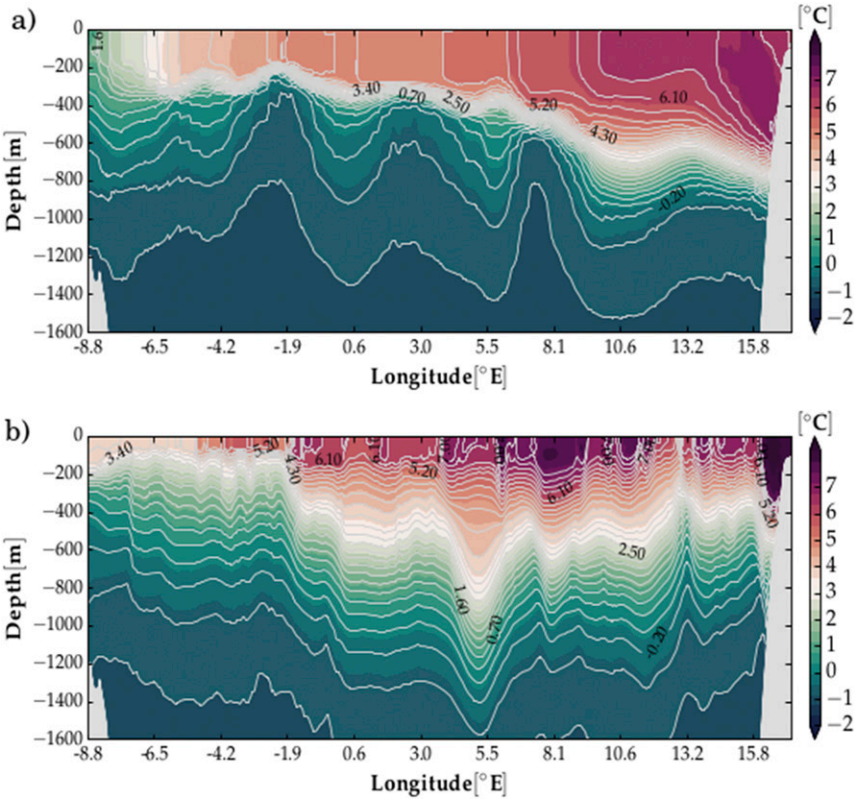

FIG. 5. Vertical transect through the basin at 70°N of model temperature taken from the initial field on (a) 15 Jan 1994 and (b) 15 Jan 2001. Temperature contours are shown in white.

Unauthenticated | Downloaded 02/18/21 11:07 AM UTC

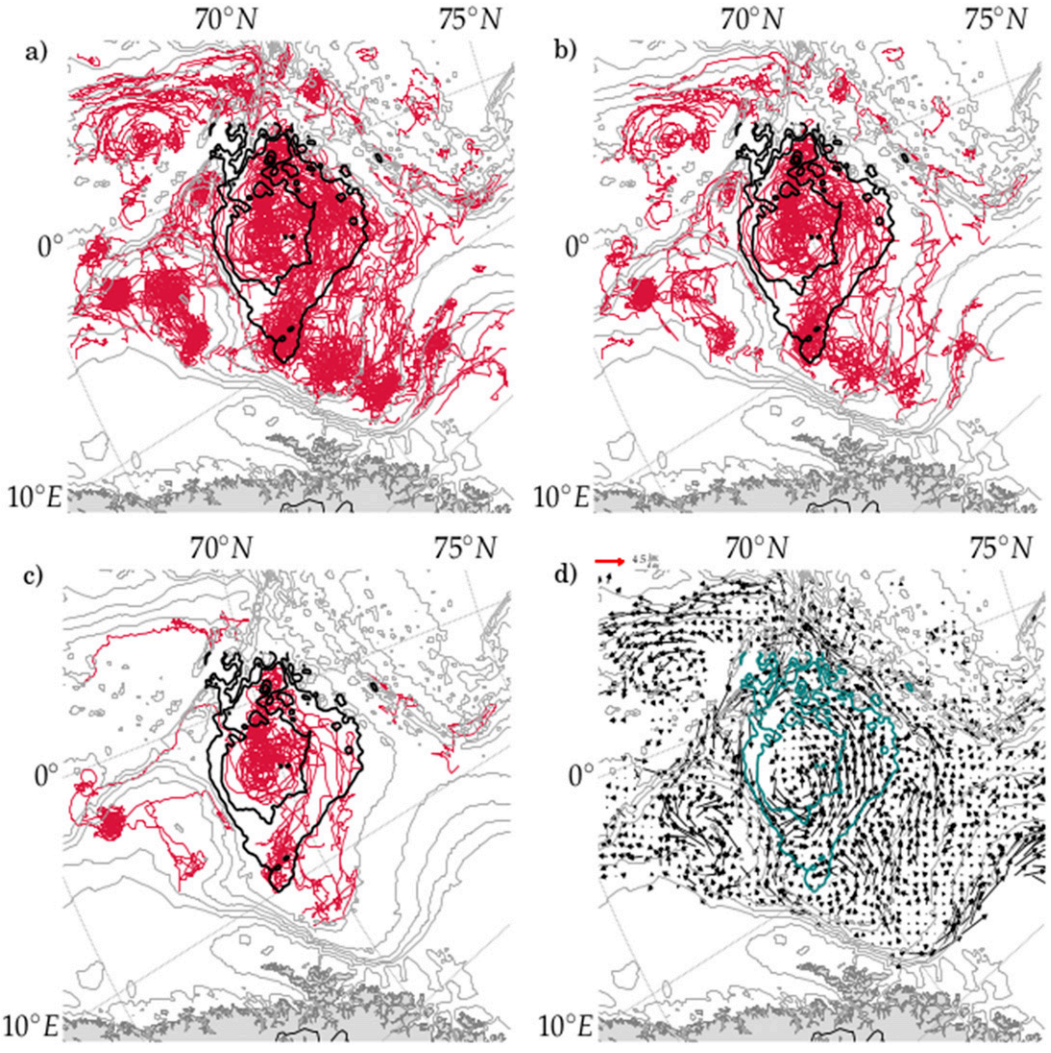

FIG. 6. (a) Anticyclonic vortex trajectories with durations longer than (a) 1, (b) 3, and (c) 7 months. (d) Binned (25 km × 25 km) vortex displacement vectors derived from these trajectories. Bins containing less than 8 counts were discarded. The 3000- and the 3200-m topographic contours surrounding the Lofoten Basin are highlighted in color. The blue box indicates a source region for anticyclonic vortex generation.

field ocean heat-flux divergence due to anticyclonic eddies propagating toward deeper waters, originating from the Lofoten continental slope, results in the general warming of upper Lofoten Basin.

Before discussing the life cycle of the Lofoten vortex in the model, we present a basin-wide census for all detected anticyclones.

b. *Propagation and hydrography of Lofoten Basin anticyclones*

Figure 6 shows the trajectories of all detected anticyclonic vortex centers that we were able to trace for 1) 1 month or longer, 2) 3 months, and 3) 7 months after the initial 2-yr spinup period. The majority of the vortices originating from the boundary current have drifted westward along cyclonically arching routes into the central Lofoten Basin. In other words, the trajectories spiral in a counterclockwise sense toward the deepest part of the basin, where they typically terminate. Longer trajectories, lasting 3–6 months, can be traced back to the slope region associated with the elevated EKE values seen in Figs. 2c and 2d, indicating a source region, shown by the blue square. Three major areas of anticyclone generation and accumulation is seen off the slope, with the associated tracks following somewhat different paths into the basin. The southernmost tracks lie right off the 3200-m isobath. Some of these break off and follow a direct route into the central Lofoten Basin, while the rest move along a curved path and then turn cyclonically later. The tracks found farther north move

Unauthenticated | Downloaded 02/18/21 11:07 AM UTC

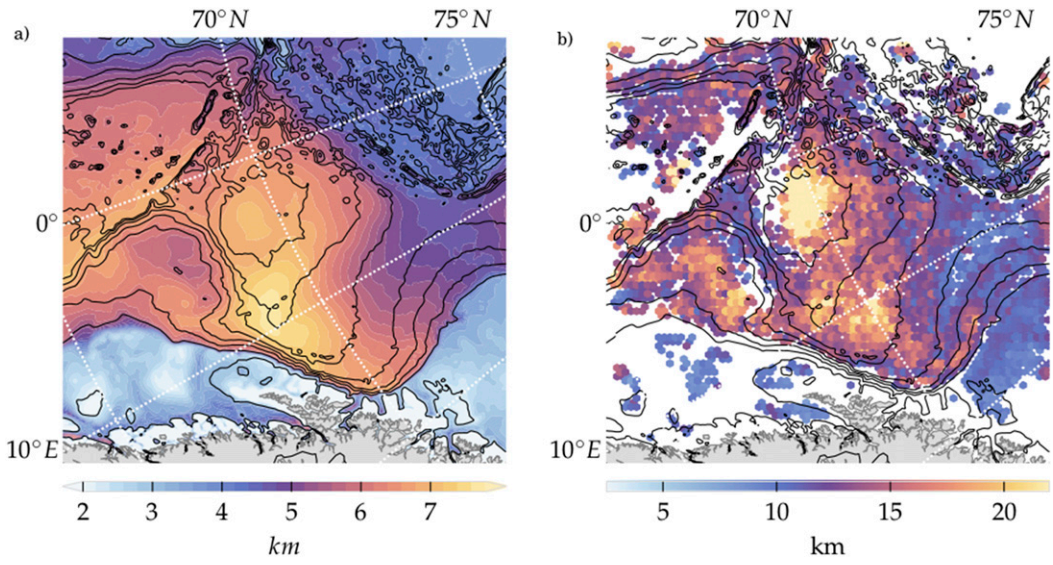

FIG. 7. (a) The first internal Rossby deformation radius ($\int_{H_0}^{0} N\,dz/f$) computed using the ambient density field and (b) vortex radii estimated from the mean distance between the eddy center and the OW contour of anticyclonic eddies. The white color indicates regions with no identified eddies.

along outer routes, tracing more or less out the 3000-m isobath. Their travel times are longer, which will likely alter their hydrographic structure. In the winter season, the vortices spending more time to reach the central basin are subject to longer cooling periods and would therefore be expected to be denser than the vortices taking the direct route from the boundary current.

Theoretical studies from the midlatitudes have shown that anticyclones tend to move southwest and cyclones to the northwest due to the planetary beta effect (McWilliams and Flierl 1979). Planetary beta effect is, however, very weak at the latitudes of the Lofoten Basin. Still, provided the slope is broad relative to the vortex length scales, the mechanism on the beta plane can be translated to vortex motion relative to topographic contours, the topographic beta effect. Taking the average magnitude of the slope within the area enclosed by the 2800-m isobath gives the following estimate of the topographic beta effect $\beta_T = f\nabla h/H \approx 2 \times 10^{-10}\,\mathrm{m^{-1}\,s^{-1}}$, which is more than an order of magnitude larger than the planetary beta effect $\beta \approx 6 \times 10^{-12}\,\mathrm{m^{-1}\,s^{-1}}$. Topographic beta causes anticyclones to propagate toward the center of a topographic depression while cyclones tend to move upslope, also moving in the pseudo-westward direction (Carnevale et al. 1991). Although their study considered barotropic vortices, we find a tendency for anticyclones to move downslope with shallow water to the right after they are released from the boundary current. The binned drift of anticyclonic tracks, shown in Fig. 6b, demonstrate a movement toward deeper regions.

The core radii of the tracked anticyclones are shown in Fig. 7b. The radii are estimated from the OW contours and radii values are bin averaged over 10 km × 10 km grid boxes. Earlier studies have shown that strong anticyclones with scales larger than the deformation radius can become very robust and have long lifetimes compared to their cyclonic counterparts. The internal Rossby radius, $L_d = \int_{-H}^{0} N\,dz/f$, computed from the model's time-mean hydrography where N is square root of the ambient buoyancy frequency, is shown in Fig. 7a. Anticyclonic vortices are here indeed generally 2–4 times larger than L_d. We also note that the distribution of radii displays some resemblance to L_d, indicating a possible linkage to linear growth theory. However, the length scales share an even stronger resemblance with the EKE field shown in Fig. 2d. Such a similarity suggests that the equilibrated eddy scales are rather set by some form of Rhines scale arrest (Held 1999; Vallis 2006), which predicts an eddy length scale on the order of $\sqrt{U/\beta}$, where U is the eddy velocity scale. If we take the topographic beta β_T and $U \sim 0.2\,\mathrm{m\,s^{-1}}$, this Rhines scale is about 30 km.

c. *Origin and characteristics of the Lofoten Basin vortex*

For the remainder of this study, we focus on the characteristics and history of the Lofoten vortex. We start by looking at a statistical description, and follow up with an investigation of the vortex life cycle.

Convection has been proposed as a generation mechanism of the LV (Ivanov and Korablev 1995b). However,

Unauthenticated | Downloaded 02/18/21 11:07 AM UTC

convection creates vertically aligned dipole vortices with cyclonic circulation in the upper ocean and anticyclonic circulation in the lower ocean (Send and Marshall 1995). Accordingly convection alone cannot create the LV, which has surface intensified anticyclonic circulation that extends to the bottom (see Fig. 9).

In our simulation, an anticyclonic vortex first appears in the center of the basin 170 days into the simulation during the spinup period. It is possible to trace this vortex back to the boundary current, in agreement with the hypothesis of Köhl (2007). On its way to the central basin, the initial LV is also subject to several mergers between smaller-scale vortices, by which it grows in size both laterally and vertically. The vertical thickness of the vortex in May is 800 m after experiencing a couple of months of winter. When it first appears near the continental slope in February–March, it is a shallow structure with a thickness of 300 m. From tracking other anticyclones throughout winter seasons, it seems doubtful that wintertime mixing alone can explain this rate of a deepening penetration of the vortex core, approximately 250 m per month. Instead, the process that allows the vortex to become a deep structure quite rapidly will be discussed in the next section.

The vortex signature grows stronger with time, following consecutive mergers after it settles in the central Lofoten Basin as the LV. From the beginning of the post spinup period, starting in 1995, a well-established anticyclonic vortex exists in the center of the basin. Close examination reveals that the LV remains coherent throughout the entire tracking period, i.e., for 8 years. The distribution of the LV positions during model years 1995–2002 are shown in Fig. 8. The time-mean position agrees well with observations (the observed location is indicated by the red cross in Fig. 1) (Fer et al. 2018). The vortex commonly resides near 2°–3°E and 69.5°–70°N, with occasional small geographical excursions. The excursions stay within the region bounded approximately by the 3200-m-depth contour. To a large extent, the shape of the distribution appears trace out the shape of the enclosing topographic contours.

Binned displacement vectors of the vortex center are also shown in Fig. 8 along with time-mean depth-averaged currents from the model. The average drift speed of the LV is about 1.7 km day^{-1}, which is close to the model-based estimate by Volkov et al. (2015) of 1.5 km day^{-1}. The vortex movement is weak with no distinct propagation direction in the deepest part of basin with the highest number of counts. This area has a fairly flat bottom topography. According to the topographic beta mechanism discussed earlier, a pseudo-westward movement is, however, evident farther out

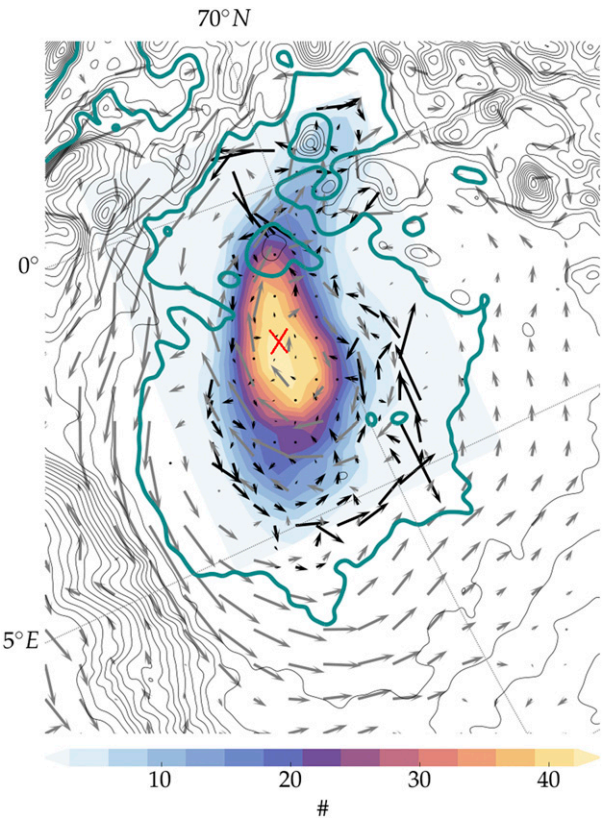

FIG. 8. Distribution of estimated LV center location (color shading) and the mean estimated center translation velocity in 15-km bins (black vectors), detected and tracked at 500-m depth over the years 1995–2003. Gray vectors show depth-average time-mean currents. Unlike earlier maps, topographic contours are drawn every 100 m in black, and the 3200-m isobath is indicated by thicker teal contours. The red cross indicates the time-mean position of the LV.

where the counts are lower. Here, the vortex might start to feel the effect of stronger topographic slopes and be forced to move cyclonically. The cyclonic drift has been mentioned in previous studies as possibly governed by the topographic beta effect (Raj et al. 2015; Søiland and Rossby 2013; Yu et al. 2017). Another possibility was suggested by Ivanov and Korablev (1995b), namely, that the LV is kept in place, within the 3000-m isobath, by its interaction with the time-mean cyclonic gyre circulation and that a cyclonic drift of the vortex center arises from the advection by the cyclonic time-mean current. The ambient depth averaged circulation simulated in the basin is indeed cyclonic, aligning with the vortex drift, and cannot be ruled out as a potential mechanism. But, importantly, the vortex drift typically exceeds the background currents, suggesting a combined effect of the topographic drift added to the advection by from the ambient circulation. The vortex detection was also carried out for cyclonic eddies (not shown here). In

Unauthenticated | Downloaded 02/18/21 11:07 AM UTC

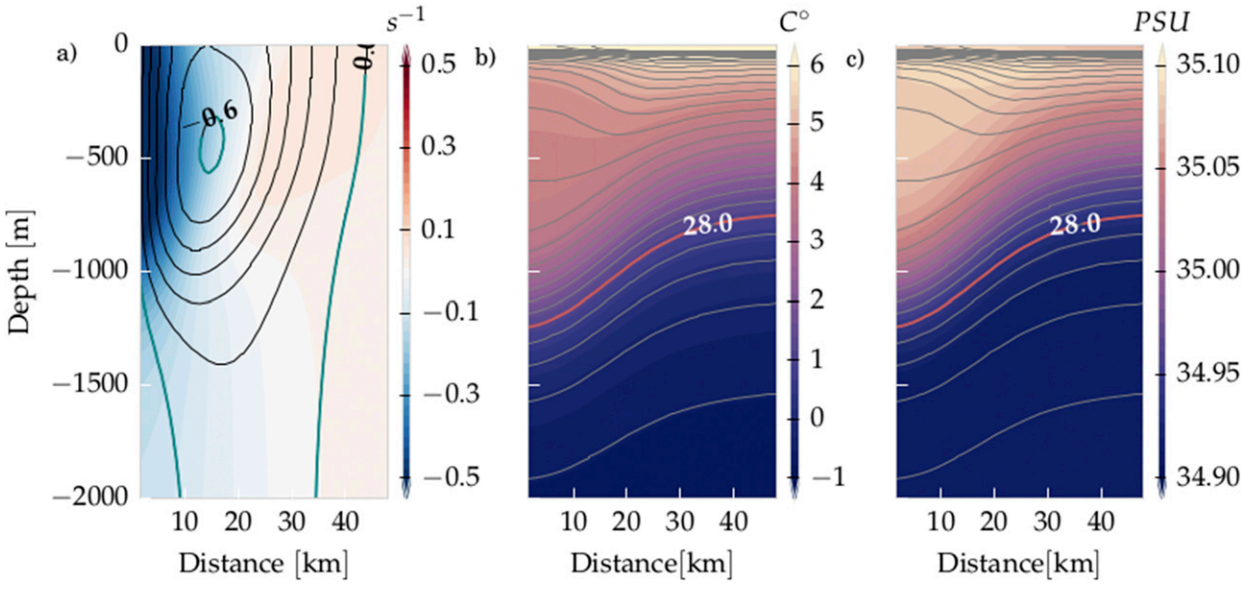

FIG. 9. Time-mean radial profiles of (a) vortex Rossby number ζ/f (color) and azimuthal velocity (black contours), with the velocity maxima and sign reversal highlighted (teal contours), (b) temperature, and (c) salinity in the Lofoten vortex core (color) together with isopycnals (gray contours). The 28.0 kg m^{-3} isopycnal is shown in red.

agreement with Köhl (2007) and Volkov et al. (2015), we found frequent occurrences of cyclonic eddies in a band around the LV. In addition to the systematic westward drift relative to topographic contours, these cyclones and other neighboring vortices will likely contribute to a chaotic component in the LV movement. From model analysis, Köhl (2007) found the drift to occur in the opposite direction, anticyclonically, and attributed this drift to the interaction with surrounding cyclonic vortices.

Figure 9 displays the LV time-mean vertical structure of azimuthally averaged properties. The vortex Rossby number ζ/f, where $\zeta = \mathbf{k} \cdot \nabla \times \mathbf{u}$ is relative vorticity, and azimuthal velocity are shown in Fig. 9a. At the center, the time-mean Rossby number reaches −0.7. The minimum instantaneous value reaches −0.94. For comparison, Yu et al. (2017) reported a minimum value of $\zeta_{\min} = -0.91\,f$ from their 3 years of Seaglider data. Similar values have been noted in other studies. With shipborne measurements, Søiland et al. (2016) estimated a minimum core vorticity of $-f$, and using 2 years of glider data Fer et al. (2018) found $\zeta_{\min} = -0.87 \pm 0.12f$. Thus our model reproduces LV core vorticity within the observed range.

The azimuthal velocity and the vorticity have pronounced subsurface maxima at a depth of about 500 m around 17 km from the center. The location roughly corresponds to the maximum isopycnal slope seen in the hydrography in Figs. 9b and 9c. The depth of the velocity maximum oscillates over time as the vortex evolves (not shown), mostly staying within the depth range of 400–900 m, and thus does at times reach the larger depth observed in other studies (Bosse et al. 2019). The maximum time-mean azimuthal velocity approaches 0.6 m s^{-1} and its peak instantaneous value exceeds 0.9 m s^{-1}. Below 1500 m, the velocity stays nearly constant, with significant bottom velocities, stronger than 0.13 m s^{-1} at 3000-m depth. Thus the vortex currents are expressed throughout the water column, and since the vortex is not isolated from the bottom, we can indeed expect bottom topography to assist in guiding the vortex movement.

d. Mergers

We will now return to the question regarding the vortex's regeneration mechanism, focusing on a time span after its formation.

Since the LV is subject to cooling periods, its core will likely exhibit different hydrographic properties than most other vortices in the basin. Figure 10 display occurrences of the density in all anticyclonic vortices identified within the 3000-m depth contour during winter and summer, respectively. Core densities, computed from vertical profiles of temperature and salinity, are extracted from the position of maximum relative vorticity in the vortex centers. The seasonal mean density of the LV core is displayed by the dashed line. The peak in occurrences at or near the dashed line reflects the LV's presence in the collection of basin vortices. The LV, being a deep and moreover denser feature, encounters anticyclones with mostly lighter cores centered on various depths but on lighter isopycnals. A vertical alignment

Unauthenticated | Downloaded 02/18/21 11:07 AM UTC

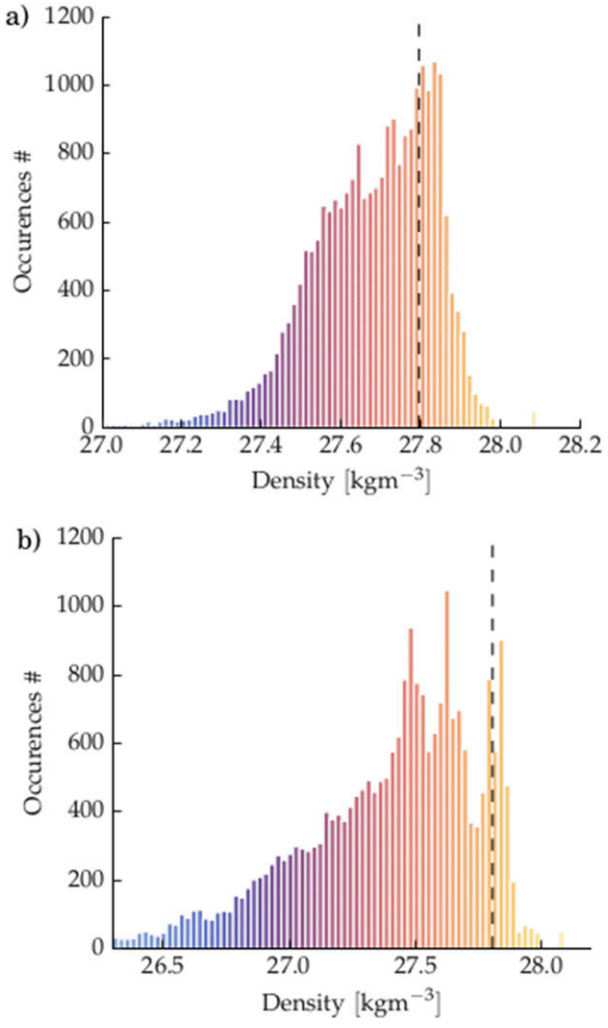

FIG. 10. Histogram of vortex core densities, extracted at depth of the maximum vorticity in the vortex center of all anticyclones identified in the central Lofoten Basin (within the 3000-m depth contour) during (a) winter and (b) summer. The dashed black lines show the time-mean density of the LV core at 400-m depth during the respective seasons.

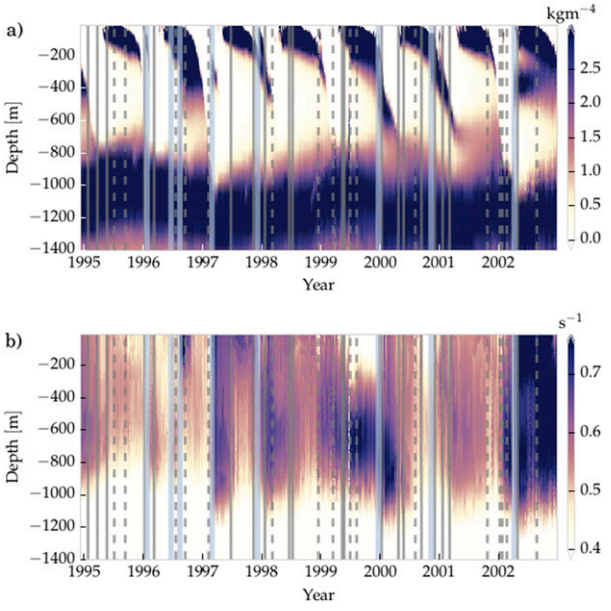

FIG. 11. Daily vertical profiles of (a) stratification and (b) absolute relative vorticity taken at the estimated LV core center. Solid gray lines mark complete merger events while dashed gray lines mark partial merger events. The translucent light blue bands denote vertical stacking events.

should then be a common outcome in the case when an encounter leads to a coalescence.

Daily vertical profiles of stratification and relative vorticity taken through the estimated center location of the LV core are shown in Fig. 11. The vertical density structure undergoes strong seasonal changes. During winter, the vortex has a well-mixed core that extends from the surface down to 800–1000 m. There is a sharp pycnocline below the core. This lower pycnocline is typically found around 1000–1200 m, in agreement with observations (Søiland et al. 2016). During summer, the LV has a lens-like signature in the density field (Fer et al. 2018). Upper and lower lobes of increased stratification create a lens-shaped subsurface structure. Starting in April/May the ocean surface experiences solar heating that puts a cap of restratified waters above the core, leading to an upper pycnocline. The surface warming extends down to approximately 200 m. When wintertime convection commences, the upper water column is again homogenized, the mixed layer grows, and the seasonal pycnocline gradually deepens. As a result of this deepening, the LV has two vertically stacked cores of weakly stratified water in early winter. In late winter, the surface undergoes strong cooling leading to vigorous vertical mixing which erodes all the way through the remains of the seasonal pycnocline, leading to the isopycnals outcropping at the surface, and the core reconnecting to atmospheric influences. The maximum depth of the summer-heated layer rarely exceeds 150–200 m, and its remnants are maintained through October/November before it deteriorates within a week due to vertical mixing.

Figure 11b show the corresponding relative vorticity profiles. These profiles do not show signs of distinct seasonal variations, but rather episodic burst of increased intensity. As there is little indication of a seasonal spinup, wintertime convection does not seem to be implicated in the main vortex regeneration. But we do not rule out a second-order impact convection might have. Next we will examine what effect merging events have on the intensity of the LV.

The conservation of potential vorticity is a key concept to consider as it is central to vortex dynamics.

Unauthenticated | Downloaded 02/18/21 11:07 AM UTC

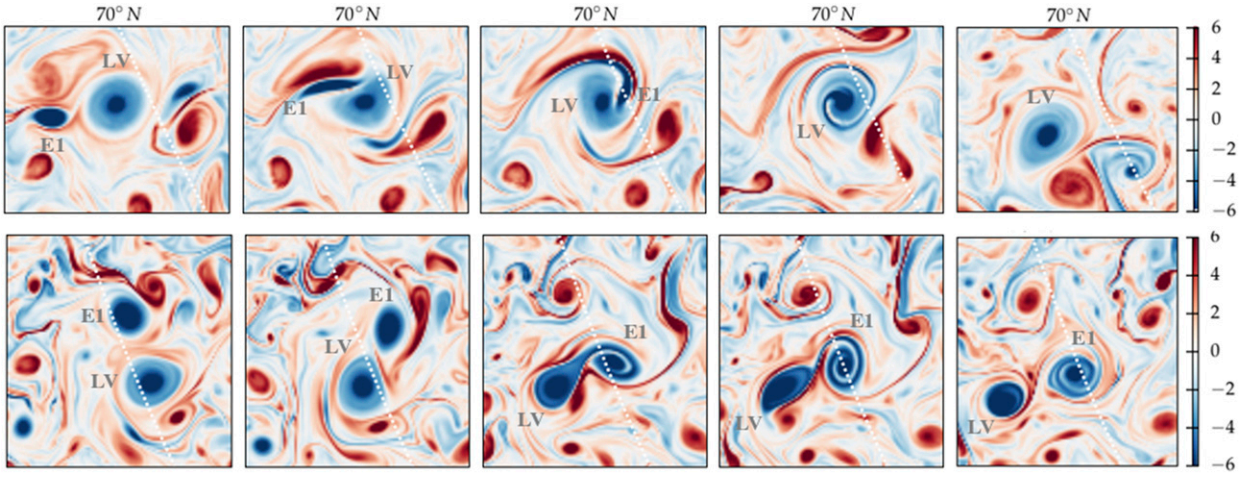

FIG. 12. Sequences of horizontal maps of relative vorticity at a 400-m depth displaying examples of (top) an asymmetric merger where the approaching vortex is smaller in size, but stronger than the LV, and (bottom) a partial merger event, where the LV is repelled from the approaching vortex after a brief interaction. The LV and the approaching vortex (E1) are labeled in all columns. The white dashed line shows 70°N.

Below, we will present the time evolution of the two main terms that constitute the quasigeostrophic potential vorticity (PV)—the stratification and the rate of spin—along the vortex trajectory. Following the vortex, in a Lagrangian framework, conservation of PV can be assumed as a first-order balance. In the absence of forcing and dissipation, the tendency equation for PV is

$$\frac{D}{Dt}q = 0,$$

$$q = \frac{\zeta + f}{\rho_0}\left(-\frac{\partial \rho}{\partial z}\right),$$

where q is the vertical component of the Ertel PV (Vallis 2006). Here ρ_0 is a reference density and $-\partial\rho/\partial z$ is a measure of the strength of the stratification. Owing to the small geographical displacements in the LV position, variations in f can be neglected. So, if the stratification increases, relative vorticity must become more negative, acting to intensify the current of an anticyclone. During violent events such as vortex mergers or in wintertime when the core is in contact with the atmosphere, we do not expect PV to be strictly conserved, but we will look for signs of correlation between two terms as we do expect to see a *tendency* toward such conservation.

Some examples of different types of mergers are shown in the horizontal vorticity maps at 500-m depth in Fig. 12. In the top row, the smaller vortex gets destroyed by LV, elongating strongly and eventually getting wrapped around it. The merger involves a neighboring cyclone that possibly assists in decreasing the separation distance between the two anticyclones. The cyclone forms a dipole with the smallest anticyclone which acts to propel it toward the LV through mutual advection. In addition to such complete merger events, the merger process is observed several times to be initiated but only partially completed. In a partial merger (PM), a filament of the weaker vortex is drained out and absorbed by the stronger vortex (Yasuda and Flierl 1995). An example of such an interaction is presented in the bottom row in Fig. 12. The southern vortex is the LV. A dipole approaches from the north, and as the separation distance between the anticyclones decrease, they start exchanging fluid. After a minor exchange, they separate. The cyclone is entrained in the interaction, and couples briefly to the LV, possibly leading to mutual advection away from the other anticyclone. It appears that the PM here leaves a more intense LV that has been reduced somewhat in size.

On average, three or four major merging events with other anticyclones are observed each year. Complete eddy merging events are marked by gray solid lines and partial merging events by gray dashed lines in Fig. 11. During some of the merging events, indicated by thicker gray bands, a double-core vertical structure suddenly appears. In such structures, two weakly stratified cores are separated by a layer of high stratification occurring at a variable depth. However, in contrast to early winter conditions, the intermediate pycnocline separating the two cores is not related to a deep seasonal pycnocline. The transition to a double-core structure is swift and is observed in all seasons, unlike the gradual, monthly transition into a double-core over the course of the winter season. This suggest a different mechanism at work. Importantly, the dividing layer is frequently deeper than the range of the seasonal pycnocline depth,

Unauthenticated | Downloaded 02/18/21 11:07 AM UTC

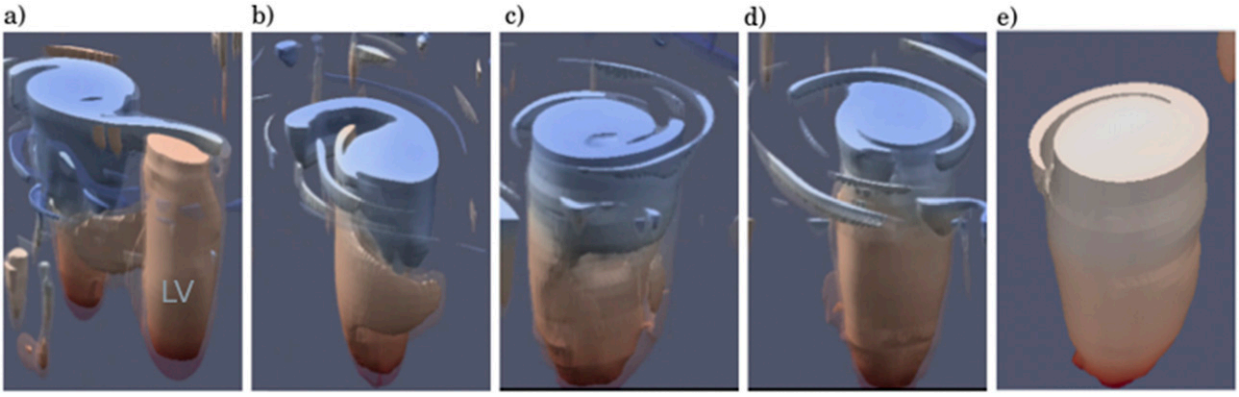

FIG. 13. (a)–(e) Isovolumes confined by the $2 \times 10^{-5}\,s^{-1}$ vorticity contour during the merger event in April/May 2002, with density shown in colors. The time from the previous plot is 12 h in (b) and (c), 10 days in (d), and 20 days in (e). The LV is labeled in (a).

situated well below 200 m. It typically persists for some months, before it erodes and the single-core structure is restored. The restoration into single vertical core happens substantially faster than when it occurs in other seasons. Occurrences of layers vertically separating two cores are evident in February 1997, December 1999, January 2000, and April 2002. Brief manifestations are also observed in January 1996 and December 1998, where initially the separation is situated around 200 m before it is shifted downward in time. Even more subtle incidents can be detected within the summer restratification caps by the staircases occurring in stratification. The most profound cases are seen in May 1996, June 1996, and October 2000. These abrupt downward shifts of stratification values are found on closer examination linked to the appearance of double cores.

The deep double-core structures arise from a vertical alignment of two anticyclones, in which one vortex slides on top of the other. Prior to the alignment the LV is 600–900 m deep. During the alignment, the core undergoes a massive vertical compression of typically 100 m or more, and from conservation of PV one would expect to see a response in relative vorticity as a result of this compression. As shown in Fig. 11b, the transitions are indeed connected to vigorous changes in relative vorticity. A rapid and substantial increase in negative vortex spin follows after a merger in all of the vertical alignment cases mentioned above. The spinup often shows a maximum increase in vorticity at around 600–700 m. However, in July 1996 only the upper part of the vortex strengthens significantly. Here, the vortex that slides on top of the LV experience greater squeezing than the LV core, while both upper and lower parts are squeezed and intensify after the January 1997 event and the April 2002 event.

Most of the partial mergers seem to have minor effects on the vortex rotation. But, there are some exceptions. Partial merger events in December 1998, June 1999 and June 2002 are all accompanied by a significant vorticity increase. The June 1999 event was illustrated in the horizontal transects in bottom panel of Fig. 12. In all cases, the cores interacting with the LV are situated on a shallower isopycnal. As they draw close to the LV, a vertical alignment is initiated but not completed. The process reaches the point at which the cores have started to compress, but no connection between the cores is established. The result is a brief interaction after which the cores detach and evolve as two separate entities, both intensified from the compression. In a fully turbulent field, it is difficult to determine what causes the vortices to separate instead of proceeding with the alignment. One speculation is that the cores may, for example, be too vertically offset, inhibiting the merger.

e. *A three-dimensional view of vertical alignment*

Next we will take a closer three-dimensional look at one instance of the vertical alignment process. We examine the alignment event with the largest impact, the spring 2002 event. Figure 13 shows isovolumes of the LV and the approaching vortex (E1) confined by the -2×10^{-5} vorticity contour at different stages of the alignment process.

The LV is well mixed throughout the core as the two vortices meet. In Fig. 13a, the two vortices approach each other and have started to corotate. In Fig. 13b, both vortices develop tentacles that extend to the other vortex. These tentacles do not evolve on the same horizontal plane. The denser vortex rather extends its tentacle below the lighter vortex's arm. As these fast-moving handles advance, they curl around the opposite vortex body allowing the vortices to latch onto each other. The deepest tentacle, from the LV, then creates a bridge to the dense part of E1, and the LV begins to submerge. The LV makes a dive and merges with the

Unauthenticated | Downloaded 02/18/21 11:07 AM UTC

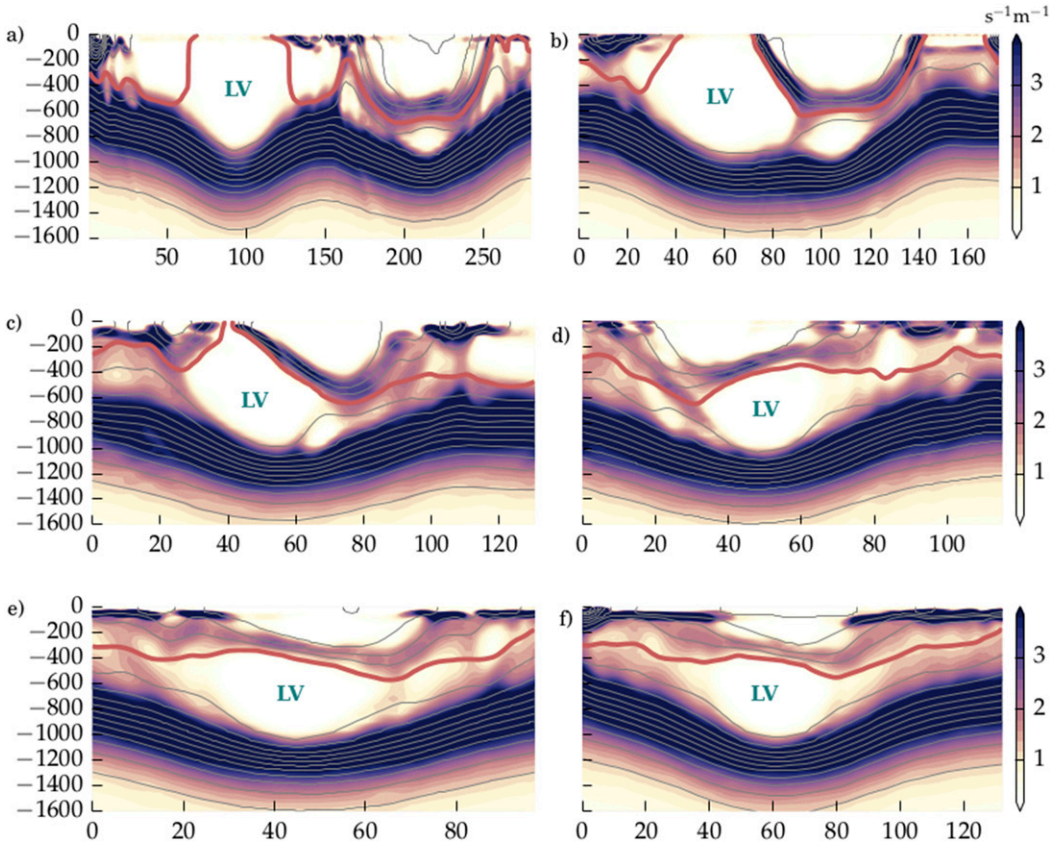

FIG. 14. Vertical transects of Ertel PV multiplied, for display purposes, by a factor of 10^{11}, taken during the April/May 2002 merger event along a line connecting the center of both vortices. Isopycnals are shown in gray contours with the 1027.82 isopycnal marked in red. Shown are day (a) 0, (b) 6, (c) 8, (d) 14, (e) 19, and (f) 24. The LV is labeled in all panels.

lower part of E1. In Figs. 13c and 13d, an adjustment process follows where the two cores wobble back and forth until they finally align about the same vertical axis. One month after the merger is initiated, in Fig. 13e, the end product is an axisymmetric double-core vortex.

The vertical motion of the vortices during the alignment is more clearly depicted in vertical transects that cut through the centers of the vortex cores. Figure 14 shows Ertel PV along such transects through the two vortex cores at different stages of the merger. The transects rotate along with the two vortices as they orbit around a common mass center. A deep structure, the LV, meets a double-core vortex, E1, of comparable size and strength. E1 was shed from the boundary current a couple of months earlier and has a lighter upper core. Prior to the LV encounter, E1 has already undergone a vertical stacking, giving it two cores separated by an intermediate pycnocline. The lower core belongs to nearly the same density class as the LV and is the remains of a basin vortex that endured the winter season. The lightest isopycnal in the LV core is highlighted by a thicker red contour, and it connects to the upper boundary of the lower E1 core. In Fig. 14b, the vortices draw near and an intersecting layer composed of high values of PV shoals and tilts toward the surface, acting as a barrier between the LV and the upper E1 core. The LV then seems to slide adiabatically under the divide, shown in Figs. 14c–e, along the isopycnal connecting it to the lower E1 core. A subsequent adjustment toward an axisymmetric structure follows in the month ahead, see Fig. 14f.

The spring 2002 merger is not unique. The winter 1997 event is very similar, for example, in that the alignment leads to a reinvigorated vortex. The resemblance is evident in Figs. 15 and 16, showing radial plots of Ertel PV and relative vorticity averaged over a 5 day period before (panels a and c) and a 5 day period after (panels b and d) the mergers. Prior to the alignment, the core is subsurface intensified centered at approximately 600 m and with a total thickness of 1000 m. After the alignment, the LV is half this thickness, having experienced massive compression in the process. The two cores

Unauthenticated | Downloaded 02/18/21 11:07 AM UTC

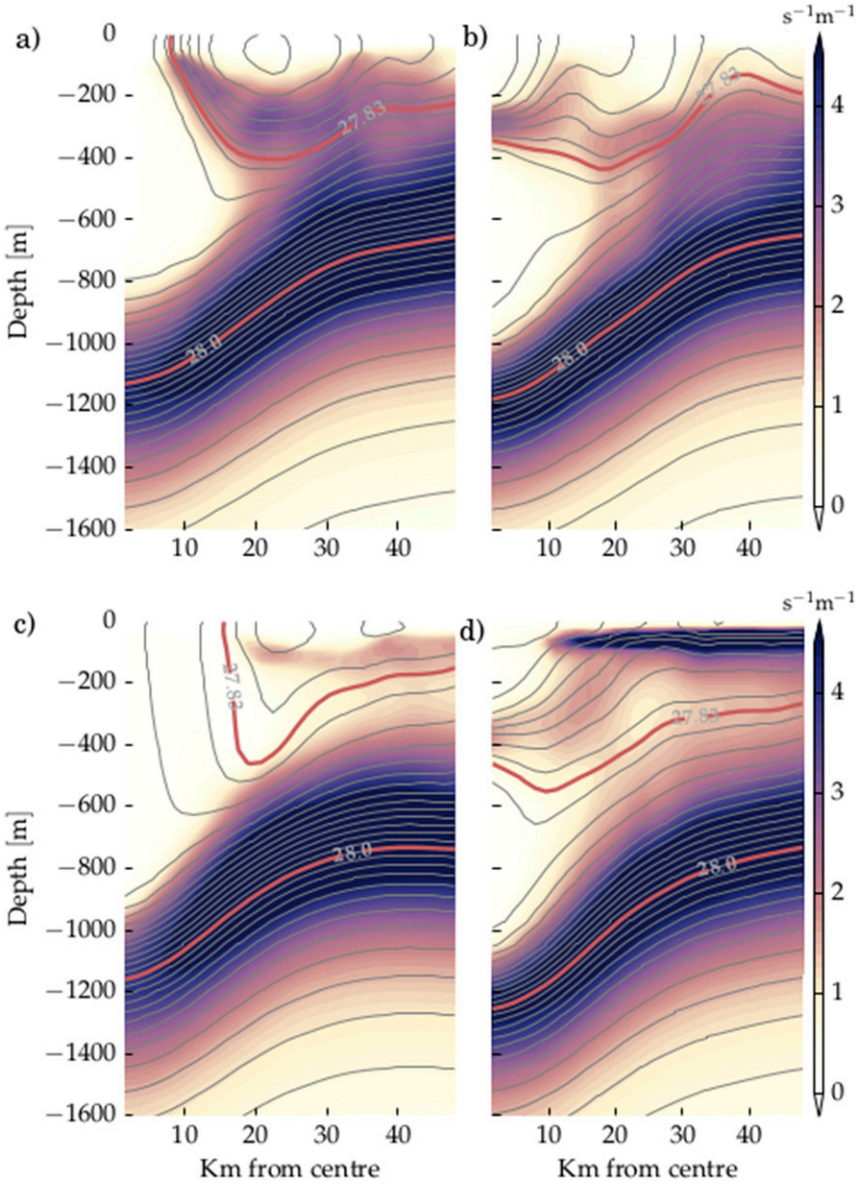

FIG. 15. Radial transects of azimuthally averaged LV Ertel PV multiplied by a factor of 10^{11}. Shown is the time mean over 5 days, (a) before and (b) after the merger in winter 1997 and (c) before and (d) after the merger in spring 2002. Density is shown in gray contours with the 1027.82 isopycnal drawn in red.

of different strengths, separated by a high PV layer, create a structure with a greater vertical extent. The 28.0 kg m^{-3} isopycnal below the initial core plunges down 100–200 m. Comparing initial and final conditions, the vorticity response is unmistakable: an upsurge in anticyclonic vortex rotation following the coalescence is clearly demonstrated.

Vertical alignment also occurs between two single-core structures. Nonetheless, the given examples serve as representative cases of the alignment process because the impact is the same even when two single cores join to share the same vertical axis. The cores are compressed and a spinup follows.

f. Integrated time series

To sum up, we present an aggregated view of the vortex evolution. Figure 17a displays a time series of volume-integrated Rossby number, Ro = ζ/f, computed from radial profiles of relative vorticity through the identified LV core. The volume of integration is bounded

Unauthenticated | Downloaded 02/18/21 11:07 AM UTC

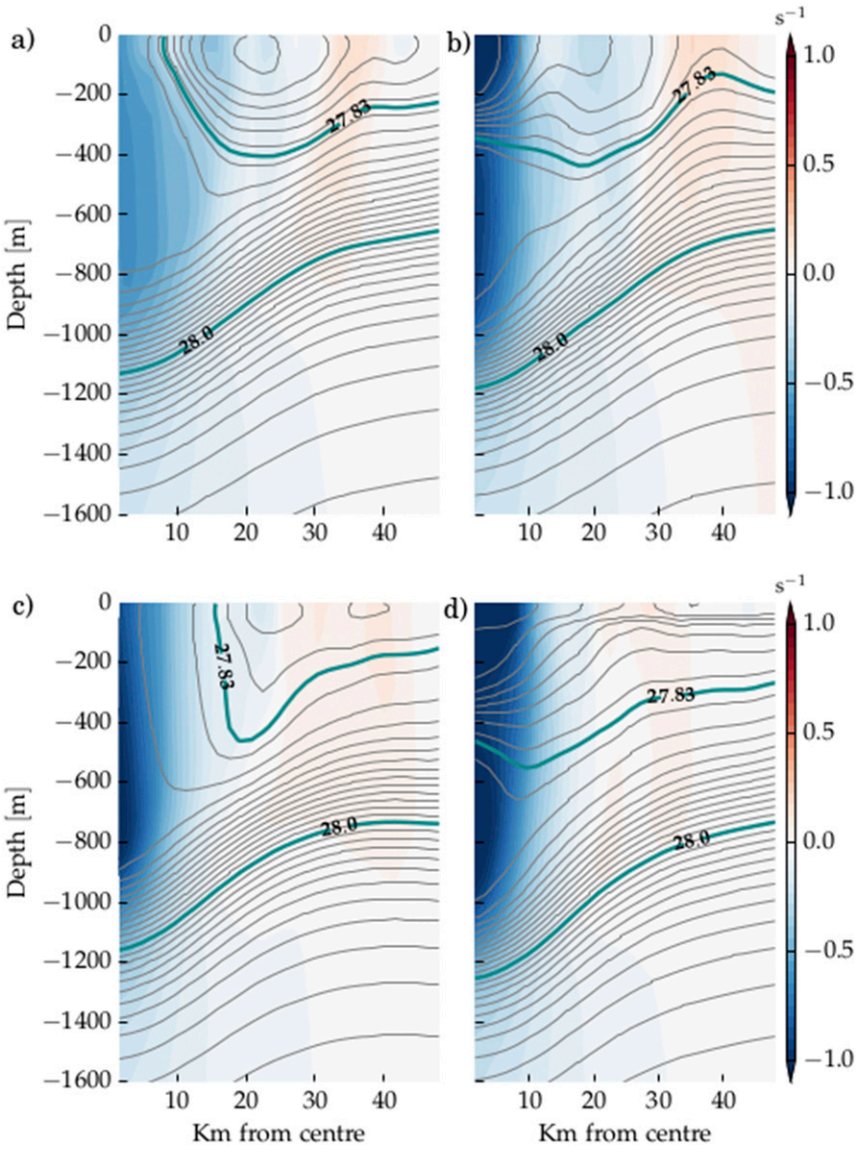

FIG. 16. Radial transects of azimuthally averaged LV relative vorticity multiplied by a factor of 10^4, and averaged over 5 days. (a) Before and (b) after the merger in winter 1997 and (c) before and (d) after the merger in spring 2002 shown in Fig. 14. Density shown as gray contours with the 1027.82 isopycnal drawn in teal. Intensification is clearly seen, as is an increase in stratification.

laterally by the vorticity sign reversal at each model level and vertically by the thickness of the vortex core. The thickness of the core is defined by the vertical distance between the 1027.795 isopycnal and the 1027.895 isopycnal. The upper isopycnal outcrops in the winter seasons. Here, complete mergers are again denoted by solid lines and PM events by dashed lines. Vertical alignments are highlighted by teal bands.

The LV vorticity varies episodically through time as seen earlier in Fig. 17a. The variations show no clear seasonal cycle. Rather, sharp bursts of increased vortex intensity accompany each vertical alignment. Generally, the peaks in vorticity are followed by a steady decay period until another reinvigoration take place. The estimated slope of the decline is a decrease of 2%–4% per month, indicating a vortex decay time of 2–5 years. Belonenko et al. (2017) found a similar decay time of 2–3 years by evaluating the change in the LV rotation in between regeneration events. They suggested either baroclinic instability or a mixed baroclinic–barotropic instability as a likely cause of the gradual decay. Primitive equation calculations showed that perturbations developed

Unauthenticated | Downloaded 02/18/21 11:07 AM UTC

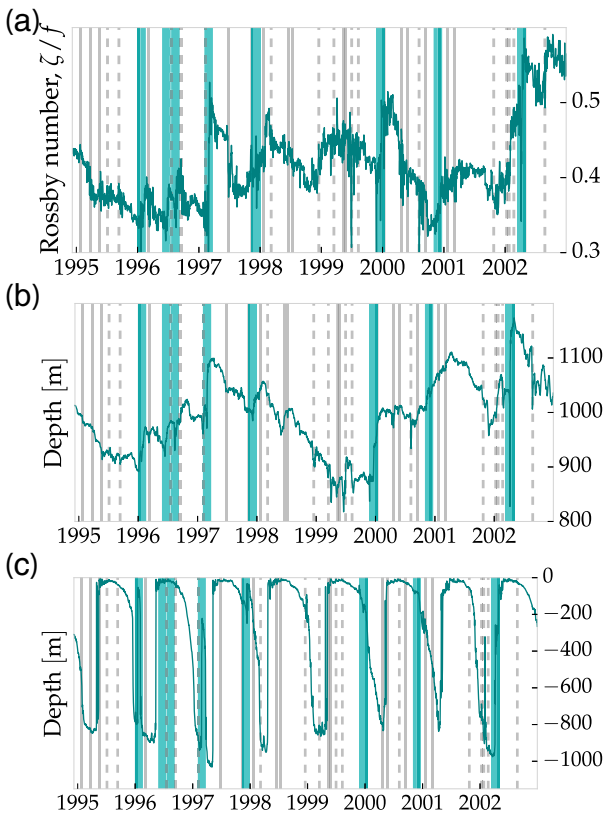

FIG. 17. Time series of (a) volume integrated Rossby number, (b) depth of the LV bottom isopycnal, and (c) LV mixed layer depth. Solid gray lines mark complete merger events, and dashed gray lines mark partial merger events. Teal bands indicate vertical alignment events.

on the rim of the vortex without penetrating deep into the core, giving rise to a decay time of 5–12 months. They noted that this time scale allowed for either eddy mergers or deep convection to interrupt further growth of the perturbations and to regenerate the LV. Finding most mergers during wintertime, they were not able to distinguish between the regeneration impact of the two mechanisms. Longer decay times have been reported in other studies considering the effect of small-scale turbulent diffusion (Søiland and Rossby 2013; Fer et al. 2018). Calculations from summertime observations suggested that the LV's total energy would be depleted in 14 years, whereas it would take 9 years for the kinetic energy to deplete (Fer et al. 2018). Our documentation of faster decay times suggests other processes are at work.

An overall gradual increase in LV Rossby number occurs during wintertime in 1998, 1999, and 2001. In 1998 and 2001, it could be linked to the vertical alignments, but there is no alignment in 1999. We are not sure why this slower, more gradual intensification occurs and we cannot exclude the possibility that convection has some impact here.

Time series of the depth of the 28.0 kg m^{-3} isopycnal, representing the bottom of the LV, is displayed in Fig. 17b. Comparing this to Fig. 17a, we see that the depth variations of LV bottom boundary largely follow the evolution of relative vorticity. In particular, depressions of this lower LV isopycnal associated with vertical alignments typically occur contemporaneously with the increases in negative relative vorticity, as expected as a consequence of the vortex alignment process.

Figure 17c shows surface mixed layer depth recorded in the LV core. The mixed layer depth is taken as the depth where $\rho_{\mathrm{MLD}} = \rho_s + 0.03\,\mathrm{kg\,m^{-3}}$, where ρ_s is the surface density at each time step. The depth of the mixed layer serves as a proxy for the strength of the wintertime convection. As discussed earlier, we do not see a clear seasonal signal in the vortex strength, as one would expect for a response to periods of convection. Specifically there is no systematic deepening of the lower vortex boundary during the winter seasons. Wintertime mixing appears commonly not to penetrate to the bottom of the vortex. Also, we note that the creation of an intermediate pycnocline through the vortex stacking act as a barrier to deep convective mixing. The role of wintertime convection thus seems mainly to act to vertically homogenize and densify the LV, rather than intensify it.

4. Discussion and conclusions

A particularly unique feature exists in the Lofoten Basin—a quasi-permanent anticyclonic vortex located in the deepest part of its topography depression. Extensive research in the area since the 1970s established the Lofoten vortex's existence and broad-scale features. However, several questions regarding the vortex's dynamics have remained outstanding. In this study we have examined in detail one of two mechanisms previously suggested for maintaining the vortex: vortex mergers (Köhl 2007). Using a model simulation with much higher resolution than previously utilized in this region has enabled us to study Lofoten vortex evolution in detail, both temporally and spatially.

The model was initialized from a coarser-resolution model simulation with fairly smooth hydrography and a weak eddy field that lacks a Lofoten Basin anticyclonic vortex. At the start of the simulation, the poleward flowing current of warm Atlantic Water along the Norwegian Continental Slope intensifies and begins to shed anticyclonic eddies that drift into the Lofoten Basin. The Lofoten vortex forms just 160–200 days into the simulation spinup, seeded by anticyclones that can

Unauthenticated | Downloaded 02/18/21 11:07 AM UTC

be traced back to the boundary current. The simulated vortex characteristics compare well with observations. The model's LV has a deep and well-mixed core with a strength in agreement with previous observational findings (Søiland and Rossby 2013; Yu et al. 2017; Fer et al. 2018). The velocity signal is found to be non-negligible at the bottom. In our model, the LV moves in a cyclonic sense at a faster rate than implied by the mean currents, suggesting topographic beta drift as an additional factor.

We found that anticyclones shed from the boundary current propagate westward and make their way into the deepest parts of the basin along generally cyclonic routes, in agreement with earlier studies (Volkov et al. 2013, 2015). Here, they interact with the LV, and some interactions lead to a coalescence. In our simulation, 3–4 merger events occur each year, with no clear seasonal bias. While there might still be favorable conditions for mergers during wintertime, we did not find this in our analysis. Köhl (2007) also found three to four yearly events. However, he observed slightly more mergers occurring during the period February–May, and none in November–December. Belonenko et al. (2017) identified one to two mergers per year with a distribution skewed toward wintertime. They analyzed the response of wintertime convection and mergers on the LV relative vorticity and energy budget. The fact that most mergers in their study happened in the same period as wintertime convection made it difficult to discern which mechanism was responsible for the vortex regeneration. They found that barotropic and baroclinic potential energy anomalies intensified during both processes, while relative vorticity did not always increase following a merger. In our analysis, the LV relative vorticity is also not affected by all mergers but importantly, it is strongly reinforced after vertical alignments. We conclude that it is these stacking events that have the strongest impact on the vortex spinup. The reinforcement take place according to the PV conservation tendency principle, through the substantial squeezing of the LV core when it is forced below a lighter core that slides on top of it. Such squeezing, on the order of hundreds of meters, was reported earlier by Cresswell (1982) in their description of the coalescence of two anticyclonic vortices in the Tasman Sea. After the alignment, the lower boundary of the lighter vortex was lifted up 230 m, while the boundary of the denser vortex was depressed by at least 100 m.

In our simulations, vertical alignment events produce a double-core structure that persists for weeks to months, depending on the season. The process we observed is well described by the experiments by Nof and Dewar (1994). A complex stacked vertical structure of the LV core has indeed been seen in observational studies (Yu et al. 2017; Fer et al. 2018). Figure 6a in Yu et al. (2017) show the radial distribution of buoyancy frequency in the LV core. The observed double core structure shown there is very similar to that found in the model following an alignment (see Figs. 15b,c). Bearing seasonal and year-to-year variations in mind, the general vertical structure of our modeled LV agrees well with the observed LV (see Figs. 3 and 4a in Fer et al. 2018). The region of strong stratification separating two cores has, however, been attributed to the remains of the seasonal pycnocline. We find that the seasonal pycnocline does not extend to a deep enough depth to explain the occasional deep occurrences of this feature, neither can it explain the sudden transition into a double-core structure.

We did not look closely into the cases where an interaction is prevented or interrupted. More studies are needed to identify criteria that allows an alignment to occur. In a study of the alignment of two three-dimensional QG vortices, Reinaud and Carton (2020) found that most vortex states are stable to vertical alignments. However, they note that alignments are indeed observed in more realistic settings, and that influences of external flow are needed for alignments to take place, because the vortices otherwise stay in stable corotating states. In our study, we saw quantitative implications of the effects of surrounding vortices during several vortex interaction events. External influences seemed to both contribute in bringing the vortices closer and, in some cases, disrupt the interaction. It seems likely that a coalescence could be interrupted by a cyclone locking onto one of the interacting anticyclones creating a dipole effect preventing further core attraction. This occurs in two of the partial merger events mentioned earlier. A dipole mechanism preventing mergers of anticyclones without a surrounding flow field was described by Ciani et al. (2016) and Valcke and Verron (1997). We were not able to observe this precise mechanism. However, we did observe a similar repulsive dipole mechanism, in the examples mentioned above, when a surrounding vortex field do exist. As pointed out by Reinaud and Carton (2020), vortex alignment in a weak internal strain field should be further addressed.

The increasing number of observations of double core oceanic eddies indicate that what has been referred to as an unusual eddy structure (Zhao and Timmermans 2015), might not be as uncommon than formerly though. Indeed, in the Labrador Sea, the number of double cores vortices observed suggested that they are more common to find than single cores in that region (Lilly et al. 2003). Among the observation sites, the most comparable region to the Lofoten Basin is possibly the Arctic Ocean. The Canada Basin, in particular, consists of closed topographic contours and is home to nearly exclusively

Unauthenticated | Downloaded 02/18/21 11:07 AM UTC

anticyclonic eddies. The bowl-shaped basin might have a similar impact as the one we see in the Lofoten Basin, where the anticyclones are attracted to the central parts. Thus, we might expect that there also exist a migration of anticyclones toward the center of the Canada Basin. In a recent study by Zhao and Timmermans (2015) 58 eddies, all anticyclones, were identified and analyzed with mooring instruments and CTD measurements. They classified three types of eddies: shallow, middepth, and deep eddies. The middepth eddies had two cores between 200 and 1000 m, and had two velocity maxima in the vertical. The two cores consisted of different water masses, the shallower core situated at the base of the halocline (≈200 m) consisted of Eurasian Water and the deeper core of Atlantic Water. The authors hypothesize that the entire eddy structure arise at the front separating Eurasian and Canadian water masses, and is then advected away from the front. While this may be an appropriate description, it is also possible, as shown in this paper, that distinct eddies that hold Eurasian and Canadian waters interact after their generation, and are forced to vertically align in a coalescence.

The LV is a special case due to its geographical stationarity and the continuous supply of anticyclones into the region. However, it is not dynamically unique in its response to an alignment. In our simulation, the dual-core structure is not only observed for the LV, but is also common for other basin anticyclones. Our results offer a clearly documented and efficient regeneration mechanism for oceanic anticyclones such as the Lofoten vortex, in which vertical alignment of a denser nucleus and a lighter satellite vortex energizes the vortex, with the two cores being subsequently fused through vertical convection.

The full picture of the Lofoten Basin vortex dynamics involves also cyclonic vortices. An extended vortex census will be presented in a follow-up study with the focus on the asymmetry between cyclones and anticyclones. The study will also present an overview of typical vertical scales and structures of the vortex field.

Acknowledgments. The Ssalto/Duacs altimeter products were produced and distributed by the Copernicus Marine and Environment Monitoring Service (CMEMS) (http://www.marine.copernicus.eu).

APPENDIX

Detection Routine

The detection routine consists of three steps. First, local extrema are identified in daily model SSH field. Each local extremum has to exceed the value of all neighboring grid points within a square box with edges 20 km from the extrema. This requirement ensures a lower limit on the separation distance between two adjacent eddies. Overestimated eddy counts will also occur less frequently since smaller-scale variations in the SSH field are ignored. Second, the largest closed SSH contour surrounding the extreme is located. Third, within the closed SSH region, we extract the OW = 0 contour. The eddy center is defined as the geographical mean position of all the points inside this OW = 0 contour. Finally, considering the finite resolution of the model, a minimum eddy effective radius is set to 2 km. Features smaller than this are rejected. A maximum eddy radius is also set to 100 km to prevent gyre-scale flows to be identified as eddies.

The effective radius of a detected vortex is estimated using the area of the OW = 0 contour, $R = \sqrt{A_{\mathrm{OW}}/\pi}$. This estimate is a conservative measure because the contour marks the extent of the inner vortex core, and will thus yield smaller vortex scales than the area of the SSH contour. Additionally, the SSH contour is often more disturbed by the nearby strain field and by the interaction with the external vortex or current field. These disturbances give rise to more variability in the size measure and stronger deformation of the contour. Laxenaire et al. (2020) shows that the contour associated with the maximum azimuthal speed, the "speed radius," is a less noisy measure of the vortex radius than that of the outermost closed SSH contour. Similarly, we find less variability in the OW contours when compared to the SSH contours. Figure 3 displays the SSH and OW contours associated with the LV extracted around the LV center during the first 4 years of the simulation. The OW contours are more compact and less elliptical, with exceptions of occasional features containing tails of high vorticity.

To follow the detected eddies in time, we use the tracking algorithm developed by Penven et al. (2005). Eddies in two subsequent daily frames are linked by a similarity condition. Two eddies, e1 and e2, are considered the same if the generalized distance

$$X_{\mathrm{e1,e2}} = \sqrt{\frac{\delta D^2}{D_0} + \frac{\delta R^2}{R_0} + \frac{\delta \zeta^2}{\zeta_0}} \tag{A1}$$

is minimal. The terms are the normalized differences in separation distance (D_0 = 25 km), radius (R_0 = 20 km), and vorticity ($\zeta_0 = 10^{-5}\,\mathrm{s}^{-1}$). To prevent a change in the vorticity signature, the normalization factor $X_{\mathrm{e1,e2}}$ is set to infinity if two eddies are of opposite polarity (Halo et al. 2014). Two eddies are not connected if the propagation distance between the

Unauthenticated | Downloaded 02/18/21 11:07 AM UTC

linked eddy positions is larger than twice the mean radius of the eddies.

During some interactions, eddies briefly share an outer SSH contour before they repel each other. In other interactions, either with the surrounding field or with other vortices, deformations cause a major distortion of the contours. The individual eddy identities are often lost during such processes. To accommodate this phenomenon, we therefore expanded the tracking routine to include a search for eddy linkages further back in time. An identified eddy is allowed to disappear for up to three days before it reappears, otherwise the track is terminated. We chose three days because by inspection this criterion showed to be stable and produce smooth trajectories, whereas for longer periods some tracks became unrealistic.

REFERENCES

Armi, L., D. Hebert, N. Oakey, J. F. Price, P. L. Richardson, H. T. Rossby, and B. Ruddick, 1989: Two years in the life of a Mediterranean salt lens. *J. Phys. Oceanogr.*, **19**, 354–370, https://doi.org/10.1175/1520-0485(1989)019<0354:TYITLO>2.0.CO;2.

Baird, M. E., and K. R. Ridgway, 2012: The southward transport of sub-mesoscale lenses of Bass Strait Water in the Centre of anti-cyclonic mesoscale eddies. *Geophys. Res. Lett.*, **39**, L02603, https://doi.org/10.1029/2011GL050643.

Barceló-Llull, B., and Coauthors, 2017: Anatomy of a subtropical intrathermocline eddy. *Deep-Sea Res. I*, **124**, 126–139, https://doi.org/10.1016/j.dsr.2017.03.012.

Beldring, S., K. Engeland, L. A. Roald, N. R. Sælthun, and A. Voksø, 2003: Estimation of parameters in a distributed precipitation-runoff model for Norway. *Hydrol. Earth Syst. Sci.*, **7**, 304–316, https://doi.org/10.5194/hess-7-304-2003.

Belkin, I., and Y. Mikhailitchenko, 1986: Thermohaline structure of the frontal zone of the northwest Pacific Ocean at 160°E (in Russian). *Okeanologiya*, **26**, 70–72.

——, A. Foppert, T. Rossby, S. Fontana, and C. Kincaid, 2020: A double-thermostad warm-core ring of the Gulf stream. *J. Phys. Oceanogr.*, **50**, 489–507, https://doi.org/10.1175/JPO-D-18-0275.1.

Belonenko, T. V., I. L. Bashmachnikov, A. V. Koldunov, and P. A. Kuibin, 2017: On the vertical velocity component in the mesoscale Lofoten vortex of the Norwegian Sea. *Izv. Atmos. Ocean. Phys.*, **53**, 641–649, https://doi.org/10.1134/S0001433817060032.

Bogdanov, K. T., V. I. Iliychev, V. B. Lobanov, and R. D. Medjitov, 1985: Investigation of anticyclonic eddy in the northwest part of the Pacific Ocean (in Russian). *Dokl. Acad. Sci. USSR*, **281**, 1210–1213.

Bosse, A., I. Fer, J. M. Lilly, and H. Søiland, 2019: Dynamical controls on the longevity of a non-linear vortex: The case of the Lofoten Basin Eddy. *Sci. Rep.*, **9**, 13448, https://doi.org/10.1038/S41598-019-49599-8.

Brundage, W. L., and J. P. Dugan, 1986: Observations of an anticyclonic eddy of 18°C water in the Sargasso Sea. *J. Phys. Oceanogr.*, **16**, 717–727, https://doi.org/10.1175/1520-0485(1986)016<0717:OOAAEO>2.0.CO;2.

Carnevale, G. F., R. C. Kloosterziel, and G. J. F. Van Heijst, 1991: Propagation of barotropic vortices over topography in a rotating tank. *J. Fluid Mech.*, **233**, 119–139, https://doi.org/10.1017/S0022112091000411.

Carton, X., N. Daniault, J. Alves, L. Cherubin, and I. Ambar, 2010: Meddy dynamics and interaction with neighboring eddies southwest of Portugal: Observations and modeling. *J. Geophys. Res.*, **115**, C06017, https://doi.org/10.1029/2009JC005646.

Chelton, D. B., M. G. Schlax, R. M. Samelson, and R. A. de Szoeke, 2007: Global observations of large oceanic eddies. *Geophys. Res. Lett.*, **34**, L15606, https://doi.org/10.1029/2007GL030812.

Ciani, D., X. Carton, and J. Verron, 2016: On the merger of subsurface isolated vortices. *Geophys. Astrophys. Fluid Dyn.*, **110**, 23–49, https://doi.org/10.1080/03091929.2015.1135430.

Cresswell, G., 1982: The coalescence of two East Australian current warm-core eddies. *Science*, **215**, 161–164, https://doi.org/10.1126/science.215.4529.161.

de Miranda, A. P., B. Barnier, and W. K. Dewar, 1999: On the dynamics of the Zapiola anticyclone. *J. Geophys. Res.*, **104**, 21 137–21 149, https://doi.org/10.1029/1999JC900042.

Dmitrenko, I. A., S. A. Kirillov, V. V. Ivanov, and R. A. Woodgate, 2008: Mesoscale Atlantic water eddy off the Laptev Sea continental slope carries the signature of upstream interaction. *J. Geophys. Res.*, **113**, C07005, https://doi.org/10.1029/2007JC004491.

Donlon, C. J., M. Martin, J. Stark, J. Roberts-Jones, E. Fiedler, and W. Wimmer, 2012: The Operational Sea Surface Temperature and Sea Ice Analysis (OSTIA) system. *Remote Sens. Environ.*, **116**, 140–158, https://doi.org/10.1016/j.rse.2010.10.017.

Fer, I., A. Bosse, B. Ferron, and P. Bouruet-Aubertot, 2018: The dissipation of kinetic energy in the Lofoten Basin eddy. *J. Phys. Oceanogr.*, **48**, 1299–1316, https://doi.org/10.1175/JPO-D-17-0244.1.

Garreau, P., F. Dumas, S. Louazel, A. Stegner, and B. Le Vu, 2018: High-resolution observations and tracking of a dual-core anticyclonic eddy in the Algerian basin. *J. Geophys. Res. Oceans*, **123**, 9320–9339, https://doi.org/10.1029/2017JC013667.

Gascard, J.-C., and K. A. Mork, 2008: Climatic importance of large-scale and mesoscale circulation in the Lofoten Basin deduced from Lagrangian observations. *Arctic-Subarctic Ocean Fluxes*, R. R. Dickson, J. Meinke, and P. Rhines, Eds., Springer, 131–143, https://doi.org/10.1007/978-1-4020-6774-7_7.

Haidvogel, D., and Coauthors, 2008: Ocean forecasting in terrain-following coordinates: Formulation and skill assessment of the regional ocean modeling system. *J. Comput. Phys.*, **227**, 3595–3624, https://doi.org/10.1016/j.jcp.2007.06.016.

Halo, I., B. Backeberg, P. Penven, I. Ansorge, C. Reason, and J. Ullgren, 2014: Eddy properties in the Mozambique channel: A comparison between observations and two numerical ocean circulation models. *Deep-Sea Res. II*, **100**, 38–53, https://doi.org/10.1016/j.dsr2.2013.10.015.

Haney, R. L., 1991: On the pressure gradient force over steep topography in sigma coordinate ocean models. *J. Phys. Oceanogr.*, **21**, 610–619, https://doi.org/10.1175/1520-0485(1991)021<0610:OTPGFO>2.0.CO;2.

Held, I. M., 1999: The macro turbulence of the troposphere. *Tellus*, **51B**, 59–70, https://doi.org/10.3402/TELLUSB.V51I1.16260.

Isern-Fontanet, J., E. García-Ladona, and J. Font, 2003: Identification of marine eddies from altimetric maps. *J. Atmos. Oceanic Technol.*, **20**, 772–778, https://doi.org/10.1175/1520-0426(2003)20<772:IOMEFA>2.0.CO;2.

Itoh, S., and I. Yasuda, 2010: Water mass structure of warm and cold anticyclonic eddies in the western boundary region of the subarctic North Pacific. *J. Phys. Oceanogr.*, **40**, 2624–2642, https://doi.org/10.1175/2010JPO4475.1.

Unauthenticated | Downloaded 02/18/21 11:07 AM UTC

Ivanov, V., and A. Korablev, 1995a: Formation and regeneration of the pycnocline lens in the Norwegian Sea. *Russ. Meteor. Hydrol.*, **9**, 62–69.

——, and ——, 1995b: Interpycnocline lens dynamics in the Norwegian Sea. *Russ. Meteor. Hydrol.*, **10**, 32–37.

Köhl, A., 2007: Generation and stability of a quasi-permanent vortex in the Lofoten Basin. *J. Phys. Oceanogr.*, **37**, 2637–2651, https://doi.org/10.1175/2007JPO3694.1.

Korablev, A., A. Smirno, and O. K. Baranova, 2014: Climatological atlas of the Nordic Seas and northern North Atlantic. NOAA Atlas NESDIS 77, 116 pp., https://data.nodc.noaa.gov/woa/REGCLIM/NORDIC_SEAS/DOC/NESDIS77-lr.pdf.

Laxenaire, R., S. Speich, and A. Stegner, 2020: Evolution of the thermohaline structure of one Agulhas ring reconstructed from satellite altimetry and Argo floats. *J. Geophys. Res. Oceans*, **124**, 8969–9003, https://doi.org/10.1029/2018JC014426.

Le Traon, P. Y., M. C. Rouquet, and C. Boissier, 1990: Spatial scales of mesoscale variability in the North Atlantic as deduced from Geosat data. *J. Geophys. Res.*, **95**, 20 267–20 285, https://doi.org/10.1029/JC095iC11p20267.

Lilly, J. M., P. B. Rhines, F. Schott, K. Lavender, J. Lazier, U. Send, and E. D. Asaro, 2003: Observations of the Labrador Sea eddy field. *Prog. Oceanogr.*, **59**, 75–176, https://doi.org/10.1016/j.pocean.2003.08.013.

MacLachlan, C., and Coauthors, 2015: Global Seasonal forecast system version 5 (GloSea5): A high-resolution seasonal forecast system. *Quart. J. Roy. Meteor. Soc.*, **141**, 1072–1084, https://doi.org/10.1002/qj.2396.

Mann, C., 1967: The termination of the Gulf Stream and the beginning of the North Atlantic Current. *Deep-Sea Res. Oceanogr. Abstr.*, **14**, 337–359, https://doi.org/10.1016/0011-7471(67)90077-0.

Mauritzen, C., 1996: Production of dense overflow waters feeding the North Atlantic across the Greenland-Scotland Ridge. Part 1: Evidence for a revised circulation scheme. *Deep-Sea Res. I*, **43**, 769–806, https://doi.org/10.1016/0967-0637(96)00037-4.

McWilliams, J. C., 1990: The vortices of two-dimensional turbulence. *J. Fluid Mech.*, **219**, 361–385, https://doi.org/10.1017/S0022112090002981.

——, and G. R. Flierl, 1979: On the evolution of isolated, nonlinear vortices. *J. Phys. Oceanogr.*, **9**, 1155–1182, https://doi.org/10.1175/1520-0485(1979)009<1155:OTEOIN>2.0.CO;2.

Meinen, C., 2001: Structure of the North Atlantic current in stream-coordinates and the circulation in the newfoundland basin. *Deep-Sea Res. I*, **48**, 1553–1580, https://doi.org/10.1016/S0967-0637(00)00103-5.

Nezlin, M. V., E. N. Snezhkin, A. Dobroslavsky, and A. Pletnev, 1993: *Rossby Vortices, Spiral Structures, Solitons: Astrophysics and Plasma Physics in Shallow Water Experiments*. Springer, 88 pp.

Nof, D., and W. Dewar, 1994: Alignment of lenses: Laboratory and numerical experiments. *Deep-Sea Res. I*, **41**, 1207–1229, https://doi.org/10.1016/0967-0637(94)90041-8.

Orvik, K. A., and P. Niiler, 2002: Major pathways of Atlantic water in the northern North Atlantic and Nordic Seas toward Arctic. *Geophys. Res. Lett.*, **29**, 1896, https://doi.org/10.1029/2002GL015002.

Penven, P., V. Echevin, J. Pasapera, F. Colas, and J. Tam, 2005: Average circulation, seasonal cycle, and mesoscale dynamics of the Peru current system: A modeling approach. *J. Geophys. Res.*, **110**, C10021, https://doi.org/10.1029/2005JC002945.

Polvani, L. M., 1991: Two-layer geostrophic vortex dynamics. Part 2. Alignment and two-layer V-states. *J. Fluid Mech.*, **225**, 241–270, https://doi.org/10.1017/S0022112091002045.

Prater, M. D., and T. B. Sanford, 1994: A meddy off Cape St. Vincent. Part I: Description. *J. Phys. Oceanogr.*, **24**, 1572–1586, https://doi.org/10.1175/1520-0485(1994)024<1572:AMOCSV>2.0.CO;2.

Raj, R., L. Chafik, J. Nilsen, T. Eldevik, and I. Halo, 2015: The Lofoten vortex of the Nordic seas. *Deep-Sea Res. I*, **96**, 1–14, https://doi.org/10.1016/j.dsr.2014.10.011.

Reinaud, J. N., and X. Carton, 2020: The alignment of two three-dimensional quasi-geostrophic vortices. *Geophys. Astrophys. Fluid Dyn.*, https://doi.org/10.1080/03091929.2019.1653462, in press.

Richardson, P. L., A. S. Bower, and W. Zenk, 2000: A census of Meddies tracked by floats. *Prog. Oceanogr.*, **45**, 209–250, https://doi.org/10.1016/S0079-6611(99)00053-1.

Rodionov, V., J. Nihoul, and A. Kostianoy, 2004: *Physical Oceanography of Frontal Zones in the Subarctic Seas*. Gulf Professional Publishing, 326 pp.

Rogachev, K., N. Shlyk, and E. Carmack, 2007: The shedding of mesoscale anticyclonic eddies from the Alaskan Stream and westward transport of warm water. *Deep-Sea Res. II*, **54**, 2643–2656, https://doi.org/10.1016/j.dsr2.2007.08.017.

Rossby, T., M. D. Prater, and H. Søiland, 2009: Pathways of inflow and dispersion of warm waters in the Nordic seas. *J. Geophys. Res.*, **114**, C04011, https://doi.org/10.1029/2008JC005073.

Schultz Tokos, K. L., H.-H. Hinrichsen, and W. Zenk, 1994: Merging and migration of two meddies. *J. Phys. Oceanogr.*, **24**, 2129–2141, https://doi.org/10.1175/1520-0485(1994)024<2129:MAMOTM>2.0.CO;2.

Send, U., and J. Marshall, 1995: Integral effects of deep convection. *J. Phys. Oceanogr.*, **25**, 855–872, https://doi.org/10.1175/1520-0485(1995)025<0855:IEODC>2.0.CO;2.

Shchepetkin, A. F., and J. C. McWilliams, 2005: The Regional Oceanic Modeling System (ROMS): A split-explicit, free-surface, topography-following-coordinate oceanic model. *Ocean Modell.*, **9**, 347–404, https://doi.org/10.1016/j.ocemod.2004.08.002.

Søiland, H., and T. Rossby, 2013: On the structure of the Lofoten Basin eddy. *J. Geophys. Res. Oceans*, **118**, 4201–4212, https://doi.org/10.1002/jgrc.20301.

——, L. Chafik, and T. Rossby, 2016: On the long-term stability of the Lofoten Basin eddy. *J. Geophys. Res. Oceans*, **121**, 4438–4449, https://doi.org/10.1002/2016JC011726.

Solodoch, A., A. Stewart, and J. C. Mcwilliams, 2020: The Mann Eddy: Formation and interaction with the North Atlantic Current. *Ocean Science Meeting*, San Diego, CA, Amer. Geophys. Union, Abstract PL24C-2676, https://agu.confex.com/agu/osm20/meetingapp.cgi/Paper/639707.

Umlauf, L., and H. Burchard, 2003: A generic length-scale equation for geophysical turbulence models. *J. Mar. Res.*, **61**, 235–265, https://doi.org/10.1357/002224003322005087.

Uppala, S. M., and Coauthors, 2005: The ERA-40 Re-Analysis. *Quart. J. Roy. Meteor. Soc.*, **131**, 2961–3012, https://doi.org/10.1256/qj.04.176.

Valcke, S., and J. Verron, 1997: Interactions of baroclinic isolated vortices: The dominant effect of shielding. *J. Phys. Oceanogr.*, **27**, 524–541, https://doi.org/10.1175/1520-0485(1997)027<0524:IOBIVT>2.0.CO;2.

Vallis, G. K., 2006: *Atmospheric and Oceanic Fluid Dynamics: Fundamentals and Large-Scale Circulation*. Cambridge University Press, 745 pp.

Unauthenticated | Downloaded 02/18/21 11:07 AM UTC

Volkov, D. L., T. V. Belonenko, and V. R. Foux, 2013: Puzzling over the dynamics of the Lofoten basin—A sub-Arctic hot spot of ocean variability. *Geophys. Res. Lett.*, **40**, 738–743, https://doi.org/10.1002/grl.50126.

——, A. Kubryakov, and R. Lumpkin, 2015: Formation and variability of the Lofoten Basin vortex in a high-resolution ocean model. *Deep-Sea Res. I*, **105**, 142–157, https://doi.org/10.1016/j.dsr.2015.09.001.

Warner, J. C., C. R. Sherwood, H. G. Arango, and R. P. Signell, 2005: Performance of four turbulence closure models implemented using a generic length scale method. *Ocean Modell.*, **8**, 81–113, https://doi.org/10.1016/j.ocemod.2003.12.003.

Yasuda, I., and G. R. Flierl, 1995: Two-dimensional asymmetric vortex merger: Contour dynamics experiment. *J. Oceanogr.*, **51**, 145–170, https://doi.org/10.1007/BF02236522.

Yu, L.-S., A. Bosse, I. Fer, K. A. Orvik, E. M. Bruvik, I. Hessevik, and K. Kvalsund, 2017: The Lofoten Basin eddy: Three years of evolution as observed by Seagliders. *J. Geophys. Res. Oceans*, **122**, 6814–6834, https://doi.org/10.1002/2017JC012982.

Zhao, M., and M.-L. Timmermans, 2015: Vertical scales and dynamics of eddies in the Arctic Ocean's Canada Basin. *J. Geophys. Res. Oceans*, **120**, 8195–8209, https://doi.org/10.1002/2015JC011251.

Unauthenticated | Downloaded 02/18/21 11:07 AM UTC